Final Technical Report

Examination of Dislocation Core Structures in B2 Intermetallic Alloys

ONR Grant Number:
N00014-90-J-1910

Martin A. Crimp, Principal Investigator
Department of Materials Science and Mechanics
Michigan State University
East Lansing, MI 48824-1226

DTIC
ELECTE
MAR 07 1995
B

DISTRIBUTION STATEMENT A
Approved for public release;
Distribution Unlimited

19950228 037

REPORT DOCUMENTATION PAGE

Form Approved
OMB No. 0704-0188

Public reporting burden for this collection of information is estimated to average 1 hour per response, including the time for reviewing instructions, searching existing data sources, gathering and maintaining the data needed, and completing and reviewing the collection of information. Send comments regarding this burden estimate or any other aspect of this collection of information, including suggestions for reducing this burden, to Washington Headquarters Services, Directorate for Information Operations and Reports, 1215 Jefferson Davis Highway, Suite 1204, Arlington, VA 22202-4302, and to the Office of Management and Budget, Paperwork Reduction Project (0704-0188), Washington, DC 20503.

1. AGENCY USE ONLY (Leave blank)	2. REPORT DATE	3. REPORT TYPE AND DATES COVERED
	27 February 1995	Final Technical Report

4. TITLE AND SUBTITLE

Examination of Dislocation Core Structures in B2 Intermetallic Alloys

5. FUNDING NUMBERS

G-N00014-90-J-1910

6. AUTHOR(S)

Martin A. Crimp

7. PERFORMING ORGANIZATION NAME(S) AND ADDRESS(ES)

Michigan State University
East Lansing, MI 48824-1226

8. PERFORMING ORGANIZATION REPORT NUMBER

9. SPONSORING/MONITORING AGENCY NAME(S) AND ADDRESS(ES)

Office of Naval Research
800 N. Quincy Street
Arlington, VA 22217-5000

10. SPONSORING/MONITORING AGENCY REPORT NUMBER

11. SUPPLEMENTARY NOTES

12a. DISTRIBUTION/AVAILABILITY STATEMENT

Available for public distribution

12b. DISTRIBUTION CODE

13. ABSTRACT *(Maximum 200 words)*

In an effort to understand the detailed mechanisms involved in the plastic deformation of crystalline materials, the atomic level structure of dislocations has been studied in B2 ordered intermetallic alloys. High resolution electron microscopy (HREM) has been used to directly image dislocation cores in NiAl, CoAl and FeAl alloys. Alloys have been studied with stoichiometric and non-stoichiometric compositions. The observed structures have been related to the mechanical behavior observed in these alloys. The experimentally observed dislocation core structures have been compared to theoretical structures modeled (under ONR support) by Prof. D. Farkas. This has led to a critical analysis of the model structures and improvement in the modeling approaches, in particular for non-stoichiometric alloys.

14. SUBJECT TERMS

Dislocation Cores, Intermetallic Alloys, NiAl, FeAl, CoAl

15. NUMBER OF PAGES

52

16. PRICE CODE

17. SECURITY CLASSIFICATION OF REPORT	18. SECURITY CLASSIFICATION OF THIS PAGE	19. SECURITY CLASSIFICATION OF ABSTRACT	20. LIMITATION OF ABSTRACT
Unclassified	Unclassified	Unclassified	

Project Summary

In an effort to understand the detailed mechanisms involved in the plastic deformation of crystalline materials, the atomic level structure of dislocations has been studied in B2 ordered intermetallic alloys. High resolution electron microscopy (HREM) has been used to directly image dislocation cores in NiAl, CoAl and FeAl alloys. Alloys have been studied with stoichiometric and non-stoichiometric compositions. The observed structures have been related to the mechanical behavior observed in these alloys. The experimentally observed dislocation core structures have been compared to theoretical structures modeled (under ONR support) by Prof. D. Farkas. This has led to a critical analysis of the model structures and improvement in the modeling approaches, in particular for non-stoichiometric alloys.

Accession For
NTIS GRA&I ☑
DTIC TAB ☐
Unannounced ☐
Justification
By
Distribution/
Availability Codes
Dist | Avail and/or Special
A-1

The primary objective of this study it to gain a better understanding of the structure of dislocations in B2 alloys and to relate this understanding to the observed mechanical behavior of these alloys. The details of this work has been documented in a number of technical papers which are included at the end of this report. This report will summarize these results by outlining the highlight of the research. Additionally, a summary of the technical presentations and research publications is included, along with a listing of the personnel involved in the program and resulting educational degrees.

INTRODUCTION

Dislocation Core Structures

It has been known for some time that the deformation behavior of materials at low to moderate temperatures is controlled by the motion of dislocations. In turn, the motion of dislocations is dictated by the atomic level structure of the dislocations. This "core structure" has thus been an area of keen interest in understanding the mechanical behavior of materials. For example, the deformation behavior of bcc metals has been rationalized [1] based on the core structure of 1/2<111> screw dislocations which relax with a three fold symmetry resulting in a non-planer structure.

The structure of dislocations cores has been examined using theoretical models such as simple pair potential models, volume dependent pair potential models and the embedded atom method. These computational approaches have been used to model dislocations in bcc, $L1_2$ and B2 alloys [2-11] resulting in a wide variety of core structures for different dislocations.

While theoretical modeling of dislocation cores in metals has been extensive, only limited experimental observations have been reported. This is due to the fact that only recently have microscopes with atomic level resolution become available. Examples of experimental studies of dislocation cores in $L1_2$ are given in [12-13]. These studies reveal that experimentally observed structures do not always agree well with predicted model structures. Thus in order to have complete confidence in the computational approach to understanding dislocation cores, more interaction between experimentalist and modelers is need.

Overview of B2 Aluminides

While the B2 intermetallic aluminides are of interest as potential materials for moderate to high temperature structural applications, these materials also make an interesting class of materials to study dislocation cores. While these materials are generally considered to have low ductilities and toughnesses at ambient temperatures, there are variations in the mechanical behavior and observed dislocations which make them of interest.

NiAl and CoAl have high moduli (230 GPa and 296 GPa respectively), and almost identical melting temperatures (1913 K and 1921 K) and lattice parameters (0.288 nm and 0.286 nm) [14]. Both of these alloys deform predominantly through the motion of <100> dislocations, with other dislocations such as <111> and <110> occasionally being observed [15-23]. However, significant differences in the mechanical behavior of these two alloys have been reported. While limited ambient temperature tensile ductilities have been reported in NiAl [24], CoAl is believed to be completely brittle at these temperatures. The most striking difference in these alloys is at higher temperatures where the creep strength of CoAl is as much as 1.5 orders of magnitude greater than NiAl [25-27]. This is despite the fact that the self diffusion rates in these alloys are

similar at the tested temperature [25], suggesting that fundamental differences in dislocation mobility may be involved. Another interesting feature of the mechanical behavior of NiAl and CoAl is that the strength increase dramatically at the composition is shifted away from the stoichiometric 50at.%Al composition [28].

The mechanical behavior of FeAl differs greatly from that observed in NiAl and CoAl. First, FeAl has its greatest strength at or near the 50at% composition. Fe-rich deviations from stoichiometry (note Al-rich deviations move the alloy out of the single B2 phase field) result in dramatic decreases in strength. In fact, substantial ductilities can be achieved in Fe-rich alloys [29]. Unlike NiAl and CoAl, the room temperature deformation is dominated by <111> dislocations in FeAl [30,31]. However, a shift to <100> slip is observed at moderate temperature [30].

Research Objectives

Because of the differences in mechanical behavior between the different B2 aluminides and because changes in stoichiometry play a significant role in the mechanical response of these materials, the objective of the present program has been to characterize the role dislocation core structure plays in the behavior of these alloys. In order to observe the core structure of these dislocations, high resolution electron microscopy [HREM] has been employed to directly image the atomic structure of some of the dislocations involved in the deformation of these alloys. It should be noted that experimental constraints of the HREM technique limit types of dislocation which can be observed. This study has focused primarily on the <100> dislocations in NiAl, CoAl and FeAl deformed at elevated temperature. In addition to stoichiometric alloys, this study has examined a number of non-stoichiometric alloys to explore the role alloy composition plays in determining the core structure.

A critical aspect of this program has been comparison of experimental images with theoretical models. Parallel to the present program, Professor D. Farkas of Virginia Polytechnic Institute has been working under an ONR grant performing EAM calculations of dislocations in these materials. Significant interaction between her group and the MSU group has taken place in order to make critical comparisons between theoretical and experimentally observed structures. Comparisons have been made by using the model structures as a basis for HREM image simulation. This has lead to considerable feedback on the modeling procedures and improvements in the modeling approaches.

RESEARCH HIGHLIGHTS

As noted above, reprints of technical papers which give the details of the present work are attached to this report. These papers include high quality images of the dislocation cores observed in this study, and consequently, additional images are not given in the body of this report. However, a written summary of the research highlights will be given.

Dislocation Cores in NiAl

The dislocation which best lends itself to core examination in NiAl alloys is the <100> edge dislocations which glide on {001} planes. The resulting line direction is a <010> type, which allows the crystalline lattice to be resolved down a low index zone while revealing the edge components of the dislocations. These <100>{001} edge dislocations are commonly observed in NiAl deformed at moderate to high temperatures, and appear to be critical to the deformation of these materials. Additionally, this same dislocation type is observed in CoAl and

FeAl alloys under various conditions, allowing comparison of the cores to be carried out in a systematic manner.

The <100>{001} edge dislocation core in stoichiometric Ni-50at%Al was found to be a compact core with no visible dissociation in to partial or fractional dislocations. That is, the dislocation has a narrow core, with most of the displacements located close to the center of the dislocation. No significant displacements normal to the slip plane were observed. When compared to the theoretical structure modeled by D. Farkas, this dislocation core is in good agreement.

In order to examine the effect of alloy stoichiometry, Ni-48at%Al and Ni-52at%Al were examined. In these cases, the <100>{001} edge dislocation cores were found to be wider, with significant displacements occurring a few atomic planes from the center of the dislocations. Also, in contrast to the cores observed in the stoichiometric alloy, substantial displacements normal to the slip plane were observed. The non-planer nature of the displacements in these cores may be associated with the increased strength and hardness in these non-stoichiometric alloys. In an effort to model these changes in structure resulting from changes in composition, D. Farkas computed cores with changes in chemistry at the center of the core, as the center of the core should be the most energetically favorable site for substitutional atoms. This approach did not however lead to changes in model core structure consistent with the experimentally observed structures. Consequently, D. Farkas has developed more complex models for off stoichiometric alloys which account for random substitutional atoms throughout the structure in addition to local chemistry changes in the core region. These more computational intensive models appear to more accurately reflect the experimentally observed structures in these non-stoichiometric alloys.

Dislocations in CoAl

Because the general aspects of deformation and dislocations in deformed single crystal B2 CoAl alloys have not been investigated previously, prior to undertaking an analysis of dislocation cores in these alloys, it was necessary to examine the general aspects of single crystal slip in these alloys. These studies revealed that many of the deformation characteristics in single crystal CoAl are similar to NiAl. However, at moderate temperatures, in addition to <100> dislocations, significant numbers of <110> and <111> dislocations are also active. At higher temperatures, <100> are typically observed forming junctions with <110> dislocations.

The <100>{001} edge dislocation cores in CoAl were in many ways similar to those observed in NiAl. In the stoichiometric Co-50at%Al alloy, the cores were again compact with no evidence of dissociation. Again, no significant displacements normal to the slip plane were observed. Thus, based on the observed structures, there are no clear reasons for the higher strength observed in CoAl. The enhance strength may be solely a result of higher bond strength which should result in increased resistance to dislocation slip.

The dislocation cores observed in the off-stoichiometric Co-Al alloys were somewhat different than those observed in the Ni-Al alloys. All of these observed cores were very compact, characterized by very narrow cores. However, like the non-stoichiometric Ni-48at%Al and Ni-52at%Al alloys, significant displacements normal to the slip plane were observed. In particular, very large displacements normal to the slip plane were observed in Co-52at%Al. It should be noted of all the alloys tested Co-52at%Al displays the highest strength.

Dislocation Cores in FeAl

The dislocation cores observed in the B2 FeAl alloys were significantly different than those observed in NiAl and CoAl. While <100>{001} edge dislocation cores were imaged, their

structures revealed significant dissociations. Some of the observed structures displayed significant glide dissociations in the {001} glide plane. However, a greater number of the observed cores revealed substantial climb dissociation components. That is, the dislocations were observed in configurations which could only be achieved by the incorporation of vacancies into the core region of the dislocation. While these structures are significantly different than those observed in CoAl and NiAl, the fact that climb dissociation is readily observed in the FeAl alloys may not be surprising. It is well known that excess thermal vacancies can lead to significant strengthening of FeAl alloys cooled from elevated temperatures [32]. However, the exact mechanism have not been clear. The results of the present study indicate that excess vacancies are easily incorporated in to the dislocations in these materials. The resulting structures are in configurations which cannot slip without re-associating into planer configurations. That is, as a result of the climb dissociation observed in the present study, the dislocations become immobile, and strengthening should be expected.

PERSONNEL

Martin A. Crimp, PI
- Supported 5% academic year, 66% summers

Scott C. Tonn
- M.S. "Dislocation Cores in B2 NiAl alloys", degree awarded 1993.

Doug Sharrott
- M.S. "High Resolution Electron Microscopy Examination of Dislocation Core Structures in B2 Fe-Al Alloys", degree awarded 1994.

Yu Zhang
- Ph.D. "Dislocations and Slip in Co-Al Alloys", Degree awarded 1995

PUBLICATIONS

D. Sharrott, Y. Zhang and M.A. Crimp, "Structural Studies of <100>{001} Edge Dislocation Cores in B2 Fe-Al Alloys", *Processing, Properties and Applications of Iron Aluminide Intermetallics*, J. Schneibel and M.A. Crimp eds., TMS Proceedings, Warrendale PA., 241 (1994).

M.A. Crimp, S.C. Tonn and Y. Zhang, "Dislocation Core Structures in B2 NiAl Alloys", Mat. Sci. and Eng., A170 (1993) pp. 95-102.

Y. Zhang, S.C. Tonn and M.A. Crimp, "Deformation Structures in Oriented NiAl and CoAl Single Crystals Deformed at Elevated Temperature", *High Temperature Intermetallic Alloys V*, I. Baker, R. Darolia and D.J. Whittenberger eds., MRS Proceedings, Vol. 288 (1993) pp. 379-384.

D. Sharrott and M.A. Crimp, "HREM Examination of Dislocation Core Structure In B2 Fe-Al Single Crystals", Mat. Sci. and Eng. (in press).

M.A. Crimp and Y. Zhang, "Characterization of Deformation Structures in B2 CoAl", *High Temperature Intermetallic Alloys VI*, Boston, J. Horton et. al. eds., MRS Proceedings, Vol. 364 (1995) (in press).

In addition, the following papers are in preparation. Copies will be forwarded to the Office of Naval Research upon publications.

Y. Zhang and M.A. Crimp, "Dislocation structures in Single Crystal CoAl deformed at Elevated Temperatues", to be submitted to Phil. Mag. A.

Y. Zhang and M.A. Crimp, "Dislocation Cores Structures in Deformed B2 Co-Al Alloys", to be submitted to Phil. Mag. A.

PRESENTATIONS

The following presentation have resulted in all or in part from the present study.

Invited Presentations

"HREM Studies of Dislocation Structures in Deformed Ordered Alloys", April 8, 1994, Virginia Polytechnic Institute and State University, Blacksburg, VA.

"HREM Studies of Dislocation Structures in Deformed Ordered Alloys", February 7, 1994, Case Western Reserve University, Cleveland OH.

"Experimental Observations of Dislocation Cores in Ordered Alloys", June 14, 1993, Department of Materials, Imperial College, London, England.

"Experimental Observations of Dislocation Cores in Ordered Alloys", June 3, 1993, Institute of Structural Metallurgy, University of Neuchatel, Neuchatel, Switzerland.

"Experimental Observations of Dislocation Cores in Ordered Alloys", June 1, 1993, Laboratoire d'Etude des Microstructures, CNRS-ONERA, Chatillon Cedex, France.

"Dislocation Core Structures in B2 Alloys," Office of Naval Research Ordered Intermetallics Conference, October 15, 1992, Annapolis MD.

"Examination of Dislocation Core Structures in B2 Intermetallic Alloys," 1991 ONR Ordered Intermetallics Meeting, June 24, 1991, Annapolis MD.

Contributed, Abstracted Presentations

"Comparison of Experimentally Observed Dislocation Structures and Theoretical Models in Intermetallic Alloys", 1995 TMS Annual Meeting, February 1995, Las Vegas NV.

"Characterization of Deformation Structures in B2 CoAl", 1994 MRS Fall Meeting, Boston MA.

"HREM Examination of <100>{001} and <110>{110} Edge Dislocations in Deformed B2 Fe-Al Single Crystals", ASM International Conference on High-Temperature Intermetallics, May 1994, San Diego CA.

"Structural Studies of <100>{001} Edge Dislocation Cores in B2 Fe-Al Alloys", 1994 TMS Annual Meeting, San Francisco CA.

"Core Structures of <100>{001} Edge Dislocations in Single Crystal CoAl", TMS 1993 Fall Meeting, Pittsburgh PA.

"HREM Study of Dislocation Structures in B2 Fe-Al Single Crystals Deformed at Elevated Temperature", TMS 1993 Fall Meeting, Pittsburgh PA.

"Deformation Structures in Oriented NiAl and CoAl Single Crystals Deformed at Elevated Temperature," 1992 MRS Fall Meeting, Boston MA.

"Dislocations in Single Crystal B2 CoAl Deformed at High Temperature," TMS 1992 Fall Meeting, Chicago IL.

"HREM Observations of [100](010) Edge Dislocations in [011] Single Crystal NiAl," TMS 1992 Fall Meeting, Chicago IL.

BIBLOGRAPHY

1. J.W. Christian, Met. Trans. A., 14A 1237 (1983).
2. V. Vitek, R.C. Perrin, and C.K. Bowen, Phil. Mag., 21 1049 (1970).
3. V. Vitek, Scripta Met., 4 725 (1970).
4. Z.S. Basinski, M.S. Duesbery, and R. Taylor, Phil. Mag., 21 1201 (1970).
5. Ibid, Can. J. Phys., 49, 2160 (1971).
6. M. Yamaguchi, *Mechanical Properties of bcc Metals*, M. Meshii ed., AIME, 31 (1981).
7. S. Takeuchi, Phil. Mag., 41A, 541 (1980).
8. M. Yamaguchi and Y. Umakoshi, *The Structure and Peroperties of Crystal Defects*, V. Paidar and L. Lejcek eds., Materials Science Monographs, 20 131.
9. S. Takeuchi, *Mechanical Properties of bcc Metals*, M. Meshii ed., AIME, 17 (1981).
10. V. Vitek, *Dislocations and Properties of Real Meterials*, Inst. of Met., London, 30 (1985).
11. M. Yamaguchi and Y. Umakoshi, Scripta Met., 9 637 (1975).
12. M.A. Crimp and P.M. Hazzledine, *High-Temperature Ordered Intermetallic Alloys III*, C.T. Liu, A.I. Taub, N.S. Stoloff and C.C. Kock eds., MRS Sym. Proc., 133 131 (1989).
13. M.A. Crimp, Phil. Mag. Let., 60 45 (1989).
14. D.L. Yaney and W.D. Nix, J. Mat. Sci., 23 3088 (1988).
15. R.J. Wasilewski, S.R. Butler, and J.E. Hanlon, Trans. AIME, 239 1357 (1967).
16. A. Ball and R.E. Smallman, Acta Met., 14 1349 (1966).
17. R.T. Pascoe and C.W.A. Newey, Met. Sci. J., 2 138 (1968).
18. I. Baker and E.M. Schulson, Met. Trans., 15A 1129 (1984).
19. M.H. Loretto and R.J. Wasilewski, Phil. Mag., 23 1311 (1971).
20. R.T. Pascoe and C.W.A. Newey, Phys. Stat. Solidi, 29 357 (1968).
21. C.H. Lloyd and M.H. Loretto, Phys. Stat. Solidi, 39 163 (1970).

22. W.D. Nix, *COSAM Program Overview*, NASA TM-83006, 183 (1982).

23. D.L. Yaney and W.D. Nix, J. Mat. Sci., 23 2083 (1986).

24. K.H. Hahn and K. Vedula, Scripta Met., 23 7 (1989).

25. L.A. Hocking, P.R. Strutt and R.A. Dodd, J. of Int. Met., 99 98 (1971).

26. J.D. Whittenberger, Mat. Sci. and Eng., 73 87 (1985).

27. J.D. Whittenberger, Mat. Sci. and Eng., 85 91 (1987).

28. J.H. Westbrook, J. Electrochem. Soc., 103 54 (1956).

29. M.A. Crimp, K.M. Vedula and D.J. Gaydosh, *High-Temperature Ordered Intermetallic Alloys II*, N.S. Stoloff, C.C. Kock, C.T. Liu and O. Izumi eds., MRS Sym. Proc., 81 499 (1987).

30. Y. Umakoshi and M. Yamaguchi, Phil. Mag. A, 41 573 (1980).

31. Ibid, 44 711 (1981)

32. M.A. Crimp and K. Vedula, Phil. Mag. A, 63 559 (1991).

Materials Science and Engineering, A170 (1993) 95–102

Dislocation core structures in B2 NiAl alloys

M. A. Crimp, S. C. Tonn and Y. Zhang

Department of Materials Science and Mechanics, Michigan State University, East Lansing, MI 48824-1226 (USA)

Abstract

Single crystals of Ni–48Al, Ni–50Al and Ni–52Al have been deformed in the [101] orientation. Slip trace and diffraction contrast Burger's vector analyses have been used to characterize the deformation characteristics of these alloys. Ni–50Al was found to display predominantly {001}⟨100⟩ slip with some limited {001}⟨100⟩ slip while the non-stoichiometric Ni–48Al and Ni–52Al exhibited a predominance of {001}⟨100⟩ slip with limited {001}⟨110⟩ dislocation motion. Direct imaging of the {001}⟨100⟩ edge dislocation cores by high resolution electron microscopy revealed differences between Ni–50Al and Ni–48Al. Cores in the Ni–48Al were found to display significantly greater spreading of the cores, both within and normal to the slip plane, than for Ni–50Al. The mechanical behavior of these alloys is rationalized in terms of these observations. Comparison of the experimental core images with simulated images based on embedded atom models of the cores indicates that the models are able accurately to predict core structures in stoichiometric alloys, but may have some limitations in predicting structures in non-stoichiometric alloys.

1. Introduction

The B2 intermetallic aluminides have received considerable attention for their potential use in high temperature corrosive environments. They possess high melting temperatures and large concentrations of Al, which make for significant weight savings and oxidation resistance. However, these B2 compounds are inhibited by their lack of ambient temperature ductility and toughness. These restrictions not only place limitations on possible applications of these materials but also inhibit the fabrication and forming capabilities of the materials which currently hinders their commercial development. This lack of toughness is the result of either an inherently low cleavage stress or the inability to initiate significant plastic flow through the activation of dislocation slip. It is of interest to gain a better understanding of the mechanisms which govern the initiation of plastic deformation and the slip of dislocations in these compounds. A better understanding of the core structure of dislocations found in these materials, specifically in NiAl, may provide a basis for the encouragement of the utilization of intermetallic aluminides. Experimental evidence of the dislocation core structure may also provide a better understanding of how the core influences the deformation properties of B2 ordered materials in general.

The motion of screw dislocations with 1/2⟨111⟩ Burger's vectors has long been known to control the mechanical behavior of b.c.c. type materials. The core structure of these screw dislocations governs the motion of these dislocations [1]. Computer models indicate that these screw dislocation cores relax with a three fold symmetry resulting in a non-planar core geometry [2–5]. In order for the dislocations to slip and cause plastic flow, this non-planar core must be transformed to a planar configuration for the dislocation to move on any given slip plane. The stress necessary to transform this core, which is directly responsible for critical resolved shear stress (CRSS), is the controlling factor in the plastic deformation.

Using pair potential models, several investigators have performed theoretical relaxations to study the core structures of the dislocations observed in B2 compounds [6–10]. The core structure of the 1/2⟨111⟩ superpartial screw dislocation in the B2 structure was found to be similar to the three fold relaxation found in the b.c.c. structure. The overall dislocation structure is made up of two 1/2⟨111⟩ dislocations separated by an antiphase boundary (APB) [6–8]. However, there is some disagreement as to which slip plane these screw dislocations slip on. ⟨111⟩ dislocations with higher APB energies have been calculated to slip on {110} planes whereas ⟨111⟩ dislocations with lower APB energies have been calculated to slip on {112} planes [6]. However, it has been observed experimentally that ⟨111⟩ dislocations slip on either {112} or {110} planes regardless of the APB energy [9]. Thus, it appears that the complex interactions between the dislocation core and APB energy are not completely understood.

⟨100⟩ and ⟨110⟩ type dislocation studies can also be found in the literature [7, 10]. Screw dislocations of these types have been found to relax in planar fashion on {011}. Hence it is expected that slip of these disloca-

0921-5093/93/$6.00

© 1993 – Elsevier Sequoia. All rights reserved

tions should be more easily activated than slip of the ⟨111⟩ screws.

Unfortunately, many dislocation models do not take into account differences in bond energy and APB energy for different B2 systems. These models are based on pair potentials of a generic B2 system [10]. However, many B2 alloys display significant differences in mechanical behavior. Some compositions such as FeAl slip with ⟨111⟩ dislocations at ambient temperatures [11–13], whereas other systems such as AuZn display ⟨100⟩ slip at room temperature [13]. Studies which take into account the individual system properties may make better predictions as to the core structure of the dislocations. For example Pasianot *et al.* [14] have used volume dependent pair potentials to determine the structure of ⟨100⟩{001} and ⟨100⟩{110} dislocations in NiAl with a variety of line directions.

Many studies have examined the slip systems activated in NiAl using slip trace analysis and electron microscopy [15–19], finding that the preferred slip systems involve ⟨001⟩ dislocations moving on {100} or {110} planes. Both edge and screw character dislocations have been observed. Some investigators have also shown the operation of ⟨111⟩ slip [20–22]. Like those in b.c.c. alloys, the ⟨111⟩ dislocations are observed as long screw dislocations with only limited edge component [21]. The ⟨111⟩ screw dislocations have been observed predominantly at low temperatures and in single crystals oriented near ⟨001⟩. The inability to observe readily these dislocations under a variety of deformation conditions suggests that they do not contribute extensively to the deformation of B2 ordered NiAl, contrary to the disordered counterpart b.c.c. A limited number of ⟨110⟩ dislocations are also observed in deformed NiAl [18, 23, 24]. Some authors believe these ⟨110⟩ dislocations slip independently [18, 23, 24]. However, others [19] suggest that these ⟨110⟩ dislocations are formed through the interaction of ⟨100⟩ type dislocations and do not contribute to the plastic deformation of NiAl.

It is the objective of the present study to examine the slip behavior of single crystal NiAl as a function of alloy stoichiometry and to image directly the core structure of the ⟨100⟩{001} edge dislocations using high resolution electron microscopy (HREM). These experimental observations will provide insight as to how the core structure influences the mechanical properties of B2 alloys.

2. Experimental procedure

Nominally stoichiometric Ni–50Al single crystals were provided by the General Electric Aircraft Engines Division, Cincinnati, OH, while Ni–48Al and Ni–52Al were provided by the Naval Air Development Center, Warminster, PA. The bulk single crystals were oriented to the [101] orientation using back reflection Laue X-ray diffraction. Gage length compression specimens were cut to a 3:1 length to width ratio and ground to 600 grit with SiC paper. The specimens were then final polished to 0.1 μm with diamond paste. Compression testing was performed at a nominal strain rate of 10^{-4} s^{-1} to approximately 5% plastic strain at 673 K in a vacuum of 10^{-5} Torr.

The active slip planes were determined by standard single crystal slip trace analysis using polarized light optical microscopy. The crystals were then sectioned parallel to the slip plane with a diamond wafering saw. Following mechanical grinding to 150 μm, specimens for TEM analysis were electropolished using a twin jet polisher operated at 12 V with a solution of one part HNO_3 to two parts methanol at a temperature of −30 °C. The dislocation Burger's vectors and line directions were determined by standard $\mathbf{g}\cdot\mathbf{b}=0$ diffraction contrast analysis and trace analysis performed on a Hitachi H-800 transmission electron microscopy operated at 200 kV.

Once the line direction and character of the dislocations were determined, another set of [101] single crystals deformed under identical conditions were sectioned perpendicular to the [010] line direction of the edge dislocations with a Burger's vector of [001] on the (100) plane. These sections were prepared by HREM examination in the same manner as outlined above. The samples were examined at 350 kV under phase contrast conditions in a JEOL 4000EX high resolution TEM to image the dislocation core structure directly.

Simulation of high resolution images of the core structure of ⟨100⟩{001} edge dislocations was performed using the EMS software package [25]. These simulations were based on embedded atom models (EAM) of dislocations in NiAl provided by D. Farkas [26]. A number of core configurations with local structure variations were simulated including stoichiometric NiAl, excess Ni, excess Al, Ni vacancy, Al vacancy and switched positions for the Ni and Al atoms. The EAM models were performed with a super cell which was two B2 cells thick in the periodic line direction of the dislocation. As a result, the local structure variations have a periodicity of twice the lattice parameter in the beam direction. For example, the Al vacancy results in every other Al atom missing at the edge of the extra half plane of the dislocation.

3. Results

The [101] compression axis was chosen for this study in an effort to enhance the cube ⟨001⟩{100} slip

with a Schmid factor of 0.5 and minimize the {001}⟨110⟩ slip with a Schmid factor of 0.354. The reasons for this will be explained later. Examination of the compressed specimens showed a number of different sets of slip lines as shown in Fig. 1. The slip trace analysis revealed the presence of up to four different active slip planes, {100}, {001}, and a number of {110} types in all of the deformed specimens. However, it is important to note that while the {110} planes appeared more dominant for the Ni–50Al, the {100} planes appeared to be more active in the non-stoichiometric Ni–48Al and Ni–52Al.

Consistent with the slip line observations, TEM analysis of the materials sectioned parallel to the (001) plane displayed a number of different dislocation types. Figure 2 displays a typical area showing the various dislocations imaged in the Ni–50Al. An analysis of the nature of these dislocations is given in Fig. 3. The substructure consists of three dislocation variants, two dislocation variants generally lying perpendicular to each other and lying in the plane of the foil, and a third type occurring in dense slip bands with the general dislocation line direction inclined to the foil. The dislocations lying in the plane of the foil have been identified (Fig. 3) as follows. The dislocations labeled a_c have a Burger's vector of [100] and a line direction of [010] and are thus pure edge dislocations. The dislocations labeled a_s also have a Burger's vector of [100] but have a zig-zag dislocation line with an average line direction of approximately [100] and thus are generally screw in nature. It would appear that these dislocations are slipping in the plane of the foil, (001). In addition to these [100] dislocations, [001] dislocations, with edge segments lying in the plane of the foil and screw segments lying perpendicular to the foil, have been observed. These dislocations would be

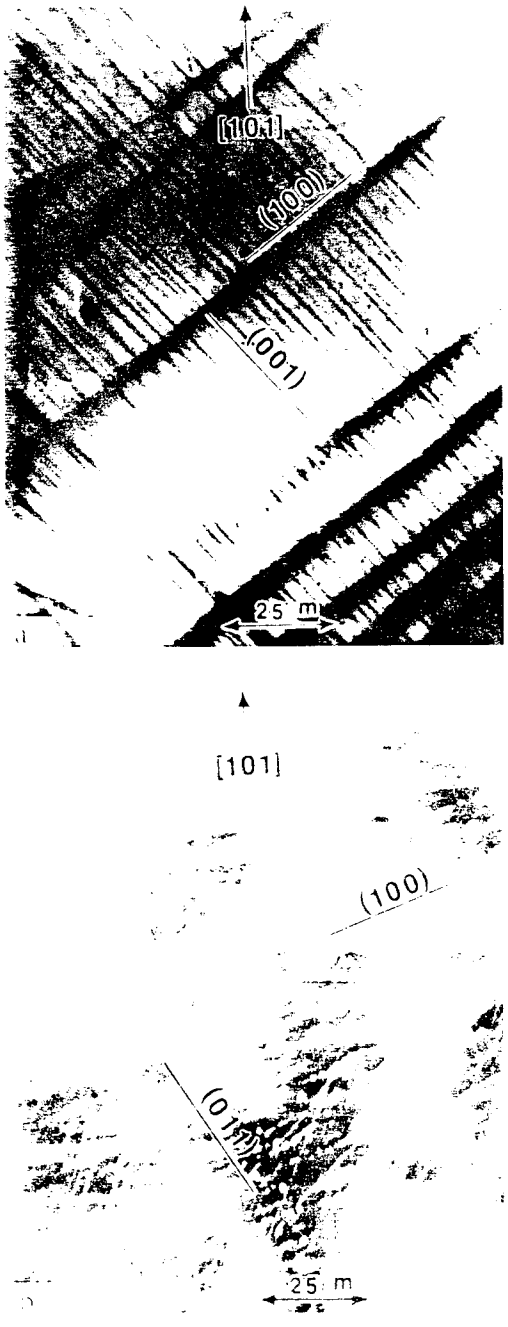

Fig. 1. Slip traces on the (a) left and (b) front faces of single crystal Ni–50Al deformed at 673 K. Trace analysis indicates slip on {001}, {100} and {101} planes.

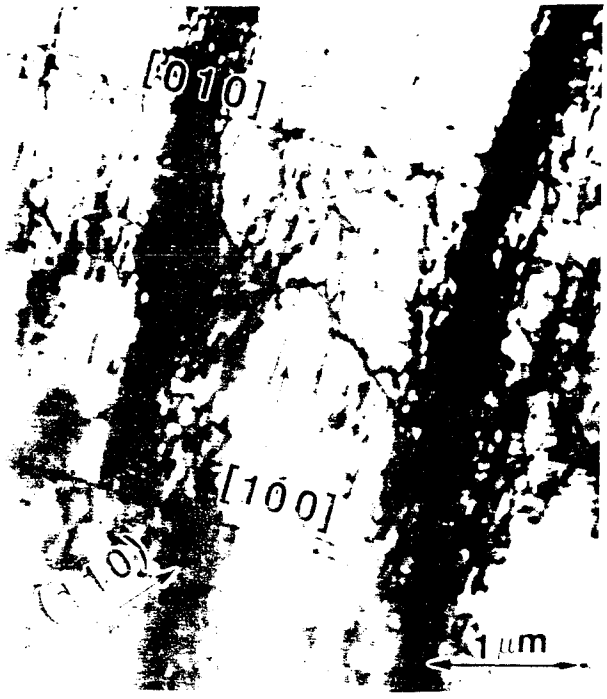

Fig. 2. Bright field electron micrograph of a (001) section of Ni–50Al displaying dislocations lying in the foil with line directions of ⟨100⟩ and ⟨010⟩ and dense slip bands of dislocations lying inclined to the foil.

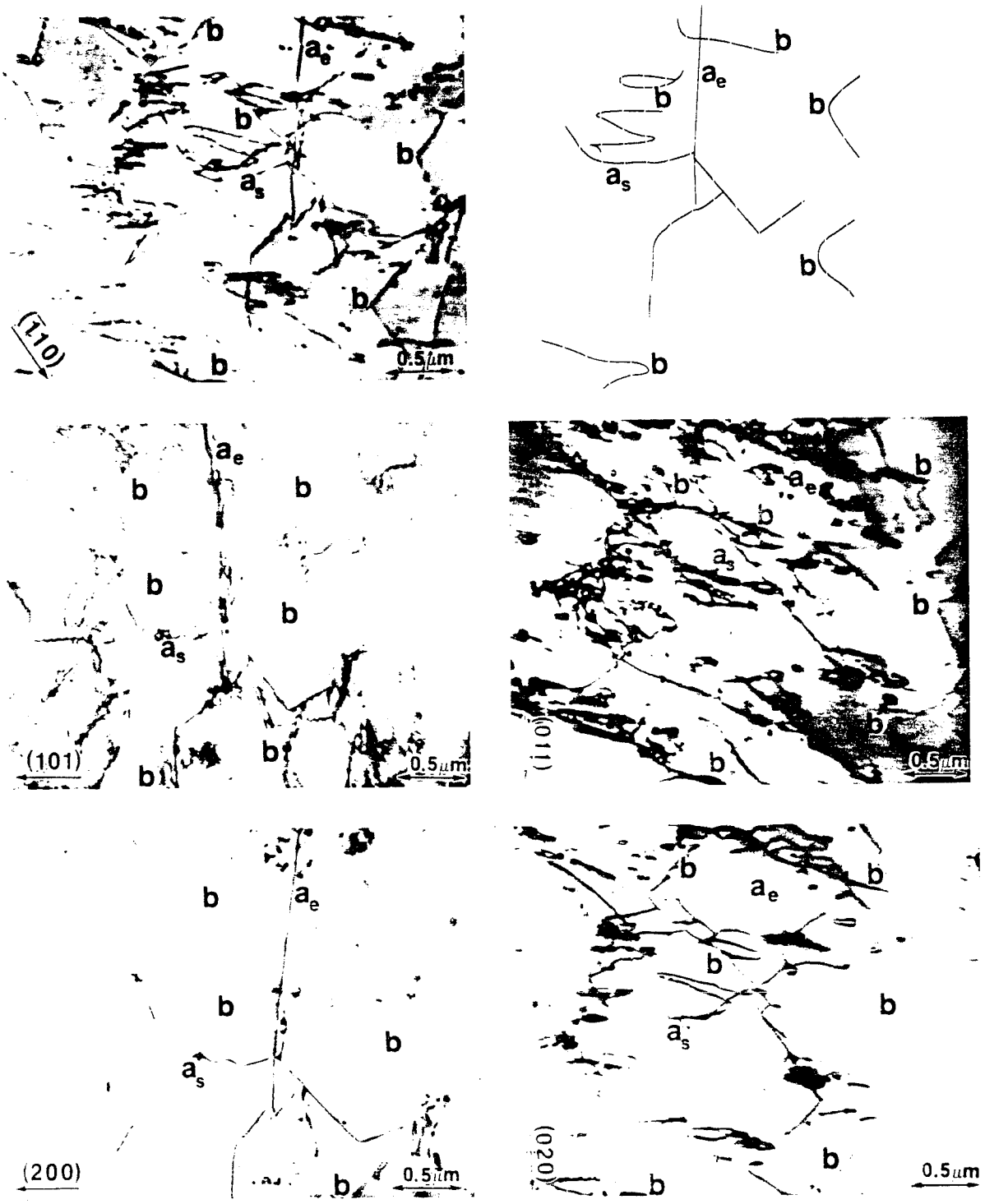

Fig. 3. Diffraction contrast analysis of the dislocations shown in Fig. 2. Edge dislocations lying in the {001} plane labeled a_e have a Burger's vector of ⟨100⟩ and a line direction of ⟨010⟩. The screw dislocations of this Burger's vector with a line direction of ⟨100⟩ are labeled a_s. Dislocations labeled b are ⟨001⟩ and/or ⟨110⟩ dislocations slipping in the {110} planes activated in the {101} orientation.

slipping in the ⟨100⟩ plane perpendicular to the plane of the foil. It has not been possible to characterize unambiguously the dislocations associated with the dense slip bands (labeled b in Fig. 3) as these dislocations show partial invisibility for a number of reflections. Presumably these are ⟨001⟩ and/or ⟨110⟩ dislocations slipping in the {110} planes observed in the slip trace analysis. The ⟨100⟩ slip band direction in the {001} TEM foil would result from the intersection of the foil with either the {01$\bar{1}$} plane or the {011}

plane, suggesting slip was occurring in either or both of these planes. Occasionally slip bands resulting from the other two {110} slip planes which are activated in the [101] orientation, (110) and (1$\bar{1}$0), are observed in the (001) foil. The relationships between the active slip planes, line directions, Burger's vectors and the plane of the foil are illustrated in Fig. 4.

Analysis of the dislocations present in the deformed Ni–48Al reveals that the same slip systems and dislocation types occur as in the stoichiometric Ni–50Al. However, consistent with the slip line observations, dislocations slipping on the ⟨001⟩ cube planes were much more prevalent than in the stoichiometric alloy. Likewise, dislocations lying on the {110} planes were not as common in the Ni–48Al alloy. The deformation structure of the Ni–52Al was similar to that observed in the Ni–48Al.

As discussed above, samples for high resolution electron microscopy were prepared by sectioning normal to the [010] direction. The reasons for this are as follows. (1) To examine a defect using HREM it is necessary for the defect to be periodic in the beam direction (the dislocation line direction must be parallel to the beam direction). (2) The defect must have significant displacement perpendicular to the beam in order to be resolved (screw components of dislocations cannot be imaged). (3) The materials must be imaged

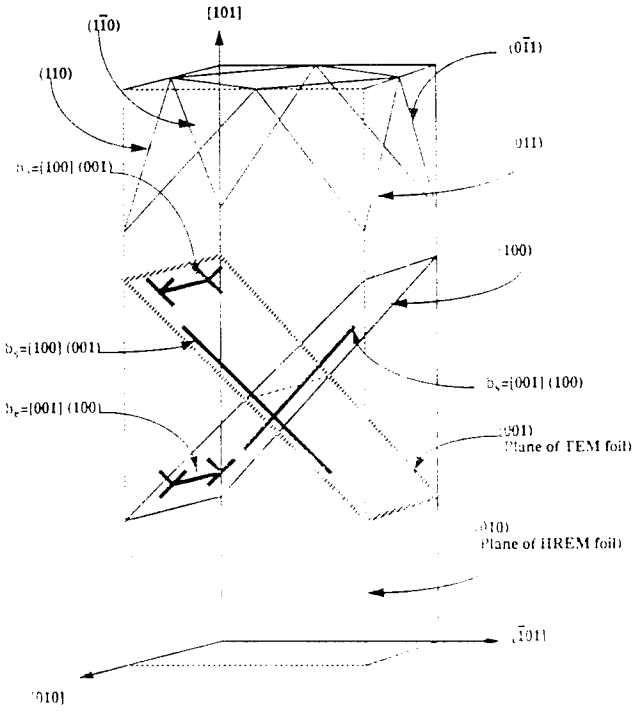

Fig. 4. Schematic representation of the single crystal compression samples illustrating the relationships between the active slip planes, dislocation line directions, Burger's vectors, the (001) TEM foil plane, and the (010) HREM foil plane.

down a low index zone such that the minimum projected interatomic spacing is greater than the resolution limit of the microscope (in this case 0.17 nm). Of the dislocations present in the deformed materials, only the (001){100} dislocations meet all of these criteria. Selection of the [010] beam direction results in both the [100](001) and [001](100) edge dislocations appearing end on. A typical bright field image of this orientation of the Ni–50Al is shown in Fig. 5(a) along with a schematic representation of the dislocation orientations in the HREM foils (Fig. 5(b)).

Phase contrast images of the ⟨001⟩ edge dislocation cores of Ni–50Al and Ni–48Al are given in Figs. 6(a) and 6(b) respectively. While both of these core structures appear at first to be similar in nature, some subtle differences can be observed. Generally, the displacements associated with the cores in the stoichiometric alloy were found to be significantly more localized than in the Ni–48Al. The spreading of the distorted core region in the slip plane is substantially wider in the non-stoichiometric Ni–48Al. Additionally, the out of plane displacements perpendicular to the slip plane and Burger's vector are much larger for this non-stoichiometric alloy. It should be noted that the structure and atomic displacements of the ⟨001⟩{100} dislocation cores in Ni–50Al agree quite well with that observed by Mills and Miracle [26] in deformed stoichiometric NiAl bicrystals.

Atomic position maps of core structures in Ni–50Al plotted from atomic positions from Farkas and Xie [27] and simulated high resolution images for conditions near Scherzer defocus are shown in Fig. 7. The representative simulations presented here correspond to the same conditions of sample thickness and defocus. The images show the differences in core structure for the changes in local stoichiometry. It is evident from the atomic displacement maps that while changes in local chemistry do result in subtle changes in the immediate vicinity of the core, there is little if any change in the displacement field more than one or two atoms distant from the core. This is reflected in the image simulations where only minor differences in the image contrast are noted in the core region as a result of changes in the local stoichiometry.

4. Discussion

It is well established that deviations from stoichiometry lead to large increases in strength of B2 NiAl alloys. This was first noted by Westbrook [28] as an increase in hardness of both Ni-rich and Al-rich NiAl relative to stoichiometric NiAl. The strengthening was attributed to defect hardening owing to either substitutional or vacancy defects which increase with devia-

Fig. 5. a Bright field electron micrograph and b schematic representation of the (010) section of Ni–50Al used for HREM. [001] {001} edge dislocations lying normal to the foil are labeled a_e. Screw orientations of these dislocations lie in the plane of the foil and are labeled a_s.

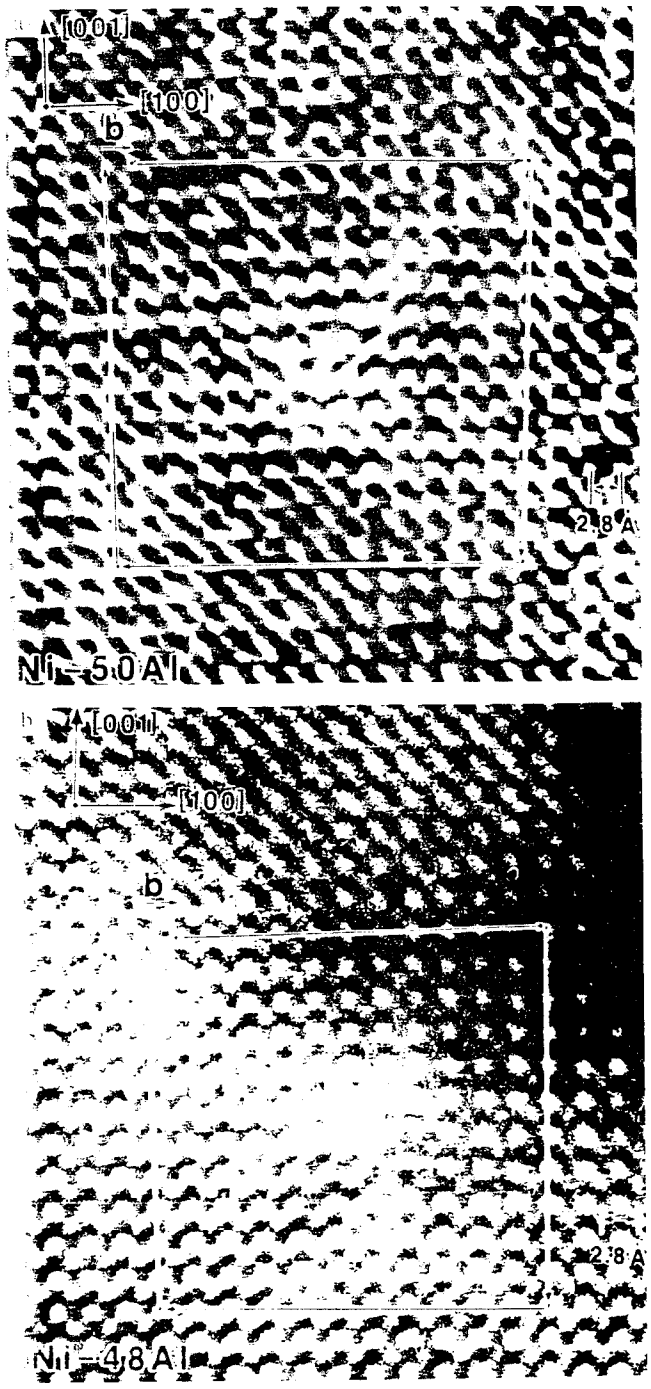

Fig. 6. HREM images of the core structures of [001] {100} edge dislocations of a Ni–50Al and b Ni–48Al.

tions from perfect stoichiometry. Following Westbrook's initial reports, Ball and Smallman [16] and Pascoe and Newey [17] found that deviations from stoichiometry dramatically increase the compressive yield strength of NiAl. Again, the strengthening was attributed to increases in point defect concentrations with non-stoichiometric Ni or Al additions. These studies led Hahn and Vedula [29] to examine the

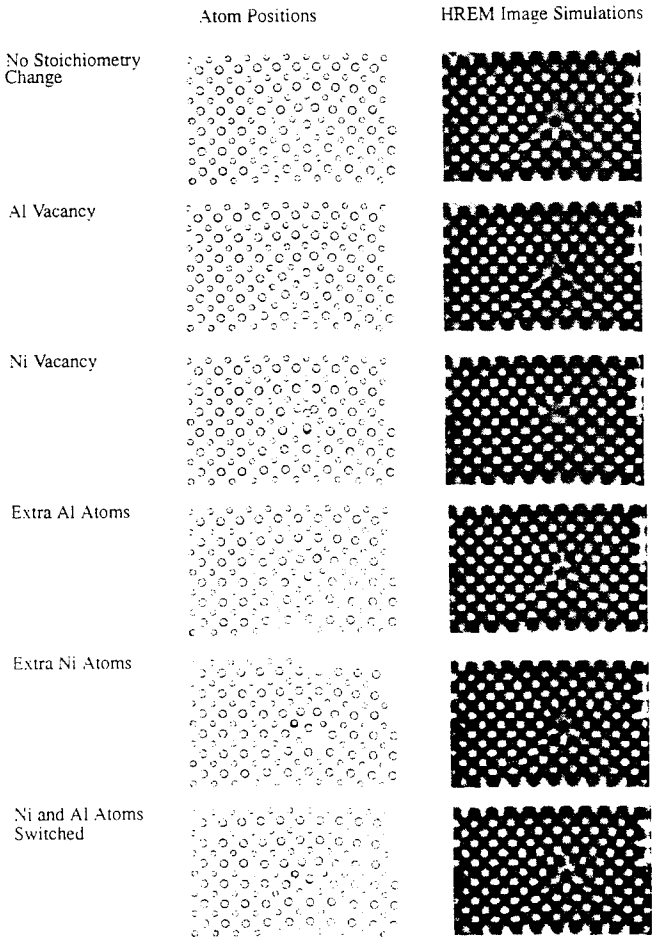

Fig. 7. Atomic position maps based on EAM calculations, and representative HREM image simulations for stoichiometric NiAl with local variations in core chemistry. Image simulations are white atom images for near Scherzer conditions corresponding to a foil thickness of 5.74 nm and a defocus of 60 nm.

tensile behavior of NiAl as a function of stoichiometry. The result was that limited tensile ductility (approximately 2%) could be achieved in essentially stoichiometric NiAl (50.3 ± 0.2 at.% Al) while non-stoichiometric alloys (47.0, 49.4, 51.3 ± 0.2 at.% Al) were essentially brittle.

The results presented in the current study may help to explain further the role of stoichiometry in the mechanical behavior of these alloys. The slip trace analysis and diffraction contrast electron microscopy observations indicate that $\langle 001 \rangle \{100\}$ slip becomes preferred over $\langle 001 \rangle \{110\}$ slip with deviations in chemistry from Ni–50Al. Of greater significance, however, is the observation of increased spreading of the dislocation core, both within the slip plane and normal to the slip plane as a result of Ni rich deviations. This change in core structure is expected to affect the critical resolved shear stress for the $\langle 001 \rangle \{100\}$ dislocations. The core relaxations in the slip plane act to increase effectively the width of the dislocation W, which is a measure of the distance of lattice distortion due to the dislocation [30]. The Peierls–Nabarro stress ($\tau_{p\text{-}n}$) dependence of the dislocation width and the Burger's vector b has been given by Hertzburg [30] as

$$\tau_{p\text{-}n} \propto Ge^{-2\pi W/b}$$

where G is the shear modulus. Thus, an increase in the spreading of the core in the slip plane would be expected to decrease the critical resolved shear stress. However, this effect may be outweighed by the effect of the core spreading normal to the slip plane. As is the case with other out of plane core dissociations [9], it will be necessary to compress the core into a planar configuration in order to initiate slip. The overall affect of the increased core spreading in Ni–48Al should be to increase the stress necessary to move the $\langle 001 \rangle \{100\}$ dislocations.

It is important to note that although the core structure of the $\langle 001 \rangle \{100\}$ dislocations observed in Ni–48Al suggests it will become more difficult to move than in the stoichiometric Ni–50Al, the slip line and diffraction contrast observations indicate that the $\langle 001 \rangle \{100\}$ dislocations in fact become easier to move relative to the other dislocations in the system. Thus while the $\langle 001 \rangle \{100\}$ dislocations are undergoing a change in core structure with stoichiometry, it may be that the other dislocations, such as the $\langle 001 \rangle \{110\}$ dislocations, are undergoing a more dramatic change in core structure which affects their mobility more significantly.

Because core structures are often studied by computer simulation techniques, it is valuable to compare the experimental observations with model structures. The atomic position maps shown in Fig. 7 show that the EAM models allow for detailed study of the fine structural changes in the cores resulting from local chemistry changes. These structural changes are somewhat apparent on the corresponding image simulations. However, when these images are compared with the experimental core images, it becomes clear that these fine details may be lost in the background noise. When the atom positions in the experimental images are carefully compared with the image simulations by overlaying images and measuring displacements, it is found that the image simulations do in fact match the core structure of the stoichiometric Ni–50Al very well. This confirms the EAM's ability to determine the overall structure of the dislocation cores in the stoichiometry alloy and the results, not only for the $\langle 001 \rangle \{100\}$ dislocations but other dislocations as well, should be accurate. Unfortunately, the EAM model has not been able to predict accurately the changes in core structure and spreading which occur as a result of deviations in alloy stoichiometry. The current model

has attempted to simulate changes in alloy stoichiometry by varying the chemistry only at the core of the dislocation. A more accurate model may be not only to vary the local core chemistry, but also to adjust the alloy stoichiometry by introducing point defects at random lattice sites throughout the entire supercell. In practice, this may be difficult to perform accurately due to the very large supercell which would be required. In the current model a supercell which was two B2 cells thick in the periodic direction of the dislocation was used for the EAM simulations. If random substitutional defects were introduced into such a supercell, the defects would, in effect, occur as defect lines in the periodic direction. To overcome this, it would be necessary to simulate a much thicker supercell in order to achieve a reasonable approximation of a random off-stoichiometric alloy. Because of the computation times involved with such a large supercell, the EAM model and other modeling techniques may not be practically suited for examining the changes in core structure which occur as a result of variations in alloy stoichiometry.

5. Conclusions

1. The deformation behavior of {101} oriented single crystal Ni–48Al, Ni–50Al and Ni–52Al has been characterized by slip trace analysis and standard diffraction contrast Burger's vector analysis. While all three compositions deform by a combination of $\langle 001 \rangle \{100\}$ and $\langle 001 \rangle \{110\}$ slip, stoichiometric Ni–50Al displays a predominance of $\langle 001 \rangle \{110\}$ slip while the non-stoichiometric alloys showed a preference for $\langle 001 \rangle \{110\}$ slip.

2. HREM imaging of the cores of $\langle 001 \rangle \{100\}$ edge dislocations revealed significantly greater spreading of the core displacements both within and normal to the slip plane for Ni–48Al than for Ni–50Al. This suggests that $\langle 001 \rangle \{100\}$ slip and possibly other dislocation slip mechanisms will be more difficult to activate in non-stoichiometric alloys.

3. Comparison of experimental core images with simulated images based on EAM models indicates that the models predict the core structure accurately for the stoichiometric alloy, but are limited in their ability to depict core structures in non-stoichiometric alloys.

Acknowledgments

This work was supported by the Office of Naval Research under grant number N00014-90-J-1910. The authors would like to thank Dr. Ram Darolia at the General Electric Aircraft Division and Mr. R. Mahapatra at the Naval Air Development Center for providing single crystals of NiAl. We would also like to thank Professor D. Farkas and Mr. Z. Xie of Virginia Polytechnic Institute and State University for providing results of their EAM calculations. The HREM was performed at the University of Michigan Electron Microbeam Analysis Laboratory, Dr. J. F. Mansfield Director.

References

1 J. W. Christian, *Metall. Trans. A, 14A* (1983) 1237.
2 V. Vitek, R. C. Perrin and C. K. Bowen, *Philos. Mag., 21* (1970) 1049.
3 V. Vitek, *Scripta Metall., 4* (1970) 725.
4 Z. S. Basinski, M. S. Duesbery and R. Taylor, *Philos. Mag., 21* (1970) 2101.
5 Z. S. Basinski, M. S. Duesbery and R. Taylor, *Can. J. Phys., 49* (1971) 2160.
6 S. Takeuchi, *Philos. Mag., 41A* (1980) 541.
7 M. Yamaguchi and Y. Umakoshi, The structure and properties of crystal defects, in V. Paidar and L. Lejcek (eds.), *Materials Science Monographs, 20* 1978, p. 131.
8 S. Tackeuchi, Mechanical properties of bcc metals, in M. Meshii (ed.), *AIME, 17* (1981).
9 V. Vitek, *Dislocations and Properties of Real Materials*, Inst. of Metals, London, 1985, p. 30.
10 M. Yamaguchi and Y. Umakoshi, *Scripta Metall., 9* (1975) 637.
11 Y. Umakoshi and M. Yamaguchi, *Philos. Mag. A, 41* (1980) 573.
12 M. A. Crimp and K. Vedula, *Philos. Mag. A, 63* (1991) 559.
13 M. H. Yoo, T. Takasugi, S. Hanada and O. Izumi, *Mater. Trans. JIM, 31* (1990) 435.
14 R. Pasianot, D. Farkas and E. J. Savino, *J. Phys. III, 1* (1991) 997.
15 R. J. Wasilewski, S. R. Butler and J. E. Hanlon, *Trans. AIME, 239* (1967) 1357.
16 A. Ball and R. E. Smallman, *Acta Metall., 14* (1966) 1349.
17 R. T. Pascoe and C. W. A. Newey, *Metall. Sci. J., 2* (1968) 138.
18 J. Bevk, R. A. Dodd and P. R. Strutt, *Metall. Trans., 4* (1973) 159.
19 I. Baker and E. M. Schulson, *Metall. Trans., 15A* (1984) 1129.
20 R. R. Bowman, R. D. Noebe and R. Darolia, *Proc. 2nd Ann. HiTemp Review*, Westlake, OH, NASA CP 10039, 1989, pp. 47–51.
21 M. H. Loretto and R. J. Wasilewski, *Philos. Mag., 23* (1971) 1311.
22 R. T. Pascoe and C. W. A. Newey, *Phys. Status Solidi, 29* (1968) 357.
23 D. B. Miracle, *Acta Metall. Mater., 39* (1991) 1457.
24 C. H. Lloyd and M. H. Loretto, *Phys. Status Solidi, 39* (1970) 163.
25 P. Stadelmann, *Ultramicroscopy, 21* (1987) 131.
26 M. J. Mills and D. B. Miracle, accepted for publication in *Acta Metall. Mater.*
27 D. Farkas and Z.-Y. Xie, personal communication.
28 J. H. Westbrook, *J. Electro. Chem. Soc., 103* (1956) 54.
29 K. H. Hahn and K. Vedula, *Scripta Metall., 23* (1989) 7.
30 R. W. Hertzberg, *Deformation and Fracture Mechanisms of Engineering Materials*, 3rd edn., J. Wiley, 1989, p. 54.

DEFORMATION STRUCTURES IN ORIENTED NiAl AND CoAl SINGLE CRYSTALS DEFORMED AT ELEVATED TEMPERATURE

Y. Zhang, S.C. Tonn and M.A. Crimp
Department of Materials Science and Mechanics, Michigan State University, East Lansing, MI 48824-1226

High Temperature Intermetallic Alloys V, I. Baker, R. Darolia and D.J. Whittenberger eds., MRS Proceedings, Vol. 288 (1993) pp. 379-384.

ABSTRACT

The deformation characteristics of the B2 intermetallic alloys NiAl and CoAl have been examined using single crystals deformed at 673 K in the <110> orientation. Slip trace analysis and transmission electron microscopy was used to characterize the deformation process. While many aspects of the deformation are similar, some distinct differences were observed. All of the alloys were found to deform by <001> slip. NiAl was found to deform by slip on a combination of {110} and {100} slip planes with the predominant slip plane being a function of alloy stoichiometry. In contrast, CoAl was found to deform by slip only on {100} planes.

INTRODUCTION

In the search for new high temperature structural materials, the B2 aluminides have received considerable attention due to their high melting temperatures, moderate densities and potential for excellent oxidation and corrosion resistance. Of these B2 alloys, NiAl has received the most attention (for review see [1]). FeAl has also received a considerable amount of research attention. However, CoAl has been the focus of very few investigations. Presumably, this is due to the reputation CoAl has for extreme brittleness.

In many respects CoAl and NiAl are very similar. Both of these materials form the B2 structure via a congruent melting point and have a wide range of solubility. The resulting structures are almost identical in terms of melting temperature (1932 K for NiAl and 1921 K for CoAl) and lattice parameter (0.288 nm and 0.286 nm respectively [2,3]). Consequently, the densities are also similar, 5.92 g/cc for NiAl versus 6.08 g/cc for CoAl [2,3] for the stoichiometric alloys.

Despite these similarities, significant differences are noted between the mechanical behavior of NiAl and CoAl. These differences were first noted by Westbrook [4] who measured the hardness of single crystals of B2 aluminides. While NiAl and CoAl both display increases in hardness with deviation in alloy stoichiometry from 50 at% Al, Westbrook found that CoAl is significantly harder than NiAl at temperatures ranging from room temperature to 1073 K. Additionally, the hardness of CoAl was found to increase at a greater rate with deviations from perfect stoichiometry. The higher hardness of CoAl is reflected in yield strength measurements recently performed by Fleisher [5] on a wide range of polycrystalline Co-Al alloys tested at temperatures up to 1223 K. When compared with similar tests for NiAl polycrystals [6,7], it is clear that the yield strength of CoAl is much greater than NiAl.

In addition to being harder and stronger than NiAl at low to moderate temperatures, CoAl also displays much greater creep strengths. Working with single crystals, Hocking, Strutt and Dodd [8] found that, depending on stress level, creep strain rates at 1323 K were at least 1.5 orders of magnitude greater in stoichiometric NiAl than stoichiometric CoAl. This is despite the fact that the diffusion rates for these alloys are very similar at this temperature [8]. In polycrystalline materials, Whittenberger [9] also found CoAl to be much more creep resistant between 1100 K and 1400 K. However, it was found that the magnitude of the

Zhang page 1 of 6

difference in creep strain rate became smaller at very high temperature [10]. These observations suggest that the enhanced creep strength of CoAl may be attributed to differences in dislocation slip behavior (and associated dislocation creep) and not the diffusional creep rate. These creep study results, along with the observed differences in hardness, indicate that there may be significant differences in the stresses necessary to initiate dislocation slip and plastic flow in these materials.

The nature of slip in B2 NiAl alloys has been studied extensively [6,11-19]. At moderate to high temperatures NiAl displays <100>{001} and <100>{011} slip, depending on orientation. If NiAl is stressed in "hard" orientations which inhibit the motion of <100> dislocations, <111> slip may be initiated at room temperature [16,20]. Additionally, <011> dislocations have been reported in NiAl [21-22], although it is not clear whether these dislocations are involved in the plastic flow or are the result of interactions of <100> dislocations.

As opposed to the large number of slip studies in NiAl, observations of dislocations in CoAl have been limited [8,23-25]. Yaney, Pelton and Nix [24] found that both <100> and <111> dislocations were present in polycrystalline CoAl extruded at 1505 K. Both the <100> and <111> dislocations were observed with long, straight segments indicating that both types were contributing to the plastic deformation [24]. Interestingly, considerable numbers of <111> edge dislocations were observed on {110} planes. This is in contrast to most bcc and ordered bcc metals, where <111> dislocations are typically observed as screw dislocations. Drelles [26] examined the deformation structures in stoichiometric CoAl single crystal deformed at room temperature. Except in orientations near <111> where some <001> slip was observed, the structure was dominated by <111> Burgers vector dislocations. No examples of <110> dislocations have been observed in CoAl.

In order to understand the pronounced differences in strength and plasticity between CoAl and NiAl, the objective of the current study is to characterize the dislocation substructure in deformed single crystal CoAl and to contrast it with that observed in deformed NiAl. This is part of a larger program devoted to the study of the dislocation core structure of B2 alloys, with the goal of understanding the differences in the mechanical properties of these materials.

EXPERIMENTAL PROCEDURE

Single crystal NiAl and CoAl, grown by the Bridgeman method, was obtained from the Naval Air Development Center and GE Aircraft Engines. The nominal composition of these alloys were Ni and Co with aluminum additions of 48, 50 and 52 atomic percent. The crystals were oriented to the [011] orientation and sectioned into 10 X 3.5 X 3.5 mm compression samples. To facilitate slip trace analysis, the specimens were mechanically polished through 0.1 μm diamond paste. Compression testing was performed at 673 K in a vacuum of 5×10^{-5} pa. The deformation was carried out at a nominal strain rate of 1×10^{-4} s^{-1} to approximately 5% plastic strain.

Standard slip trace analysis was performed on the deformed samples to determine the active slip planes. Sections were then taken parallel to the slip plane for TEM thin foil preparation. Thin foils were prepared by thinning in a twin jet electropolisher. NiAl samples were prepared using a solution of two parts methanol to one part HNO_3 at -30°C under a potential of 12 volts. The CoAl foils were electropolished at -20°C in a solution of 10% perchloric acid in methanol at 10 volts.

The deformation structures were characterized using standard diffraction contrast techniques including $\mathbf{g} \cdot \mathbf{b} = 0$ analysis. The dislocation line directions, slip planes and Burger's vectors were determined.

RESULTS AND DISCUSSION

The [011] orientation was chosen for the compression axis in this study in an effort to enhance <001>{100} slip for the purposes of dislocation core examination. Unfortunately, this orientation may lead to slip on a number of different planes as two <001>{100} slip systems and/or up to four <001>{110} slip systems may be activated. The slip trace analysis of the deformed NiAl single crystals revealed the presence of both duplex {100} and {101} slip planes (Fig. 1). In the stoichiometric Ni-50Al, the {110} planes appeared to be dominant, whereas in the off-stoichiometric Ni-48Al and Ni-52Al, the {001} planes appeared to be the most active. In contrast, only duplex {001} slip was observed in all of the CoAl alloys as shown in Figure 2. In these alloys, the primary effect of off-stoichiometric deviations in chemistry was to decrease the overall amount of observed slip. This was particularly true for the Co-48Al where it was difficult to

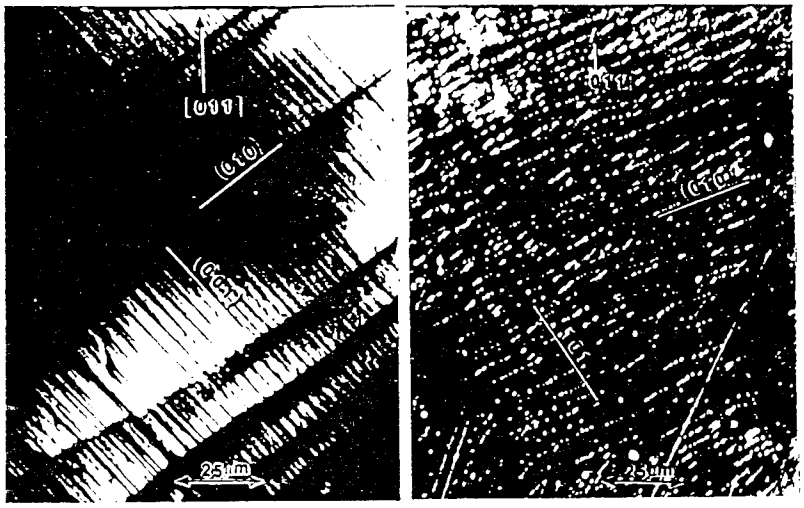

Figure 1. Examples of slip lines on two perpendicular faces of deformed stoichiometric <110> NiAl single crystal.

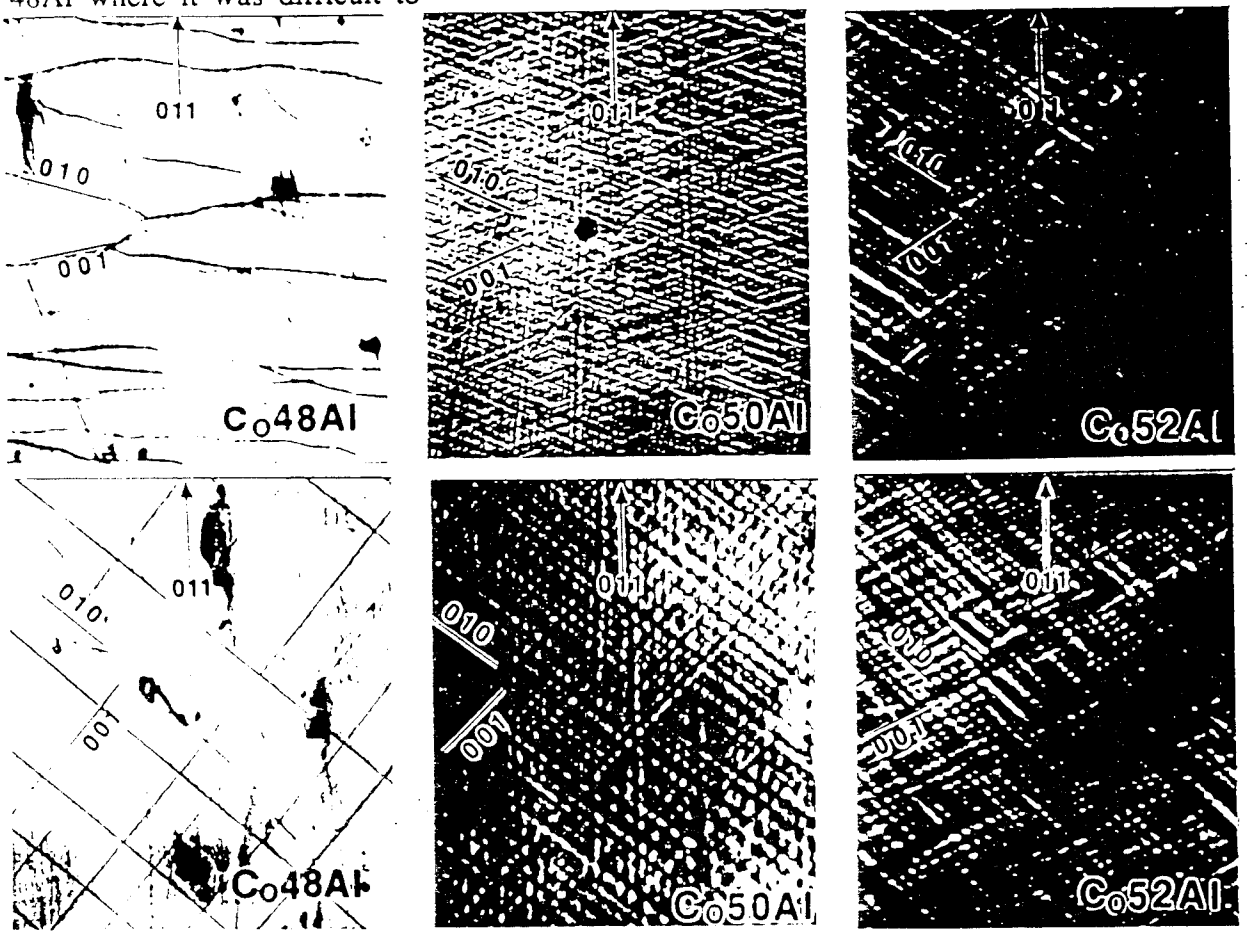

Figure 2. Examples of slip lines on two perpendicular faces of <110> single crystal CoAl with various alloy stoichiometries.

deform the materials beyond 2% plastic strain. This behavior corresponds to the increases in hardness observed with increased deviation in alloy stoichiometry [4]. In all of the Co-Al compression samples, a significant kinking was observed.

TEM examination of sections parallel to the {001} slip planes revealed a number of different dislocation configurations in the stoichiometric Ni-50Al as illustrated in Figure 3. Two types of long straight dislocations lying within the plane of the foil with line directions of [100] and [001] were observed. Additionally, heavy dense bands of dislocations inclined to the foil, with an overall band direction in the foil of [001] were observed. Diffraction contrast $\mathbf{g}\cdot\mathbf{b}=0$ analysis revealed the straight dislocations lying in the plane of the foil were [001] and [010] dislocations with either pure edge or pure screw orientations. These dislocations would have moved primarily on the {100} slip planes. The inclined dislocations in the thick deformation bands were found to also have [010] Burgers vectors. These dislocations which were predominantly mixed in character were presumably slipping on the (110) plane.

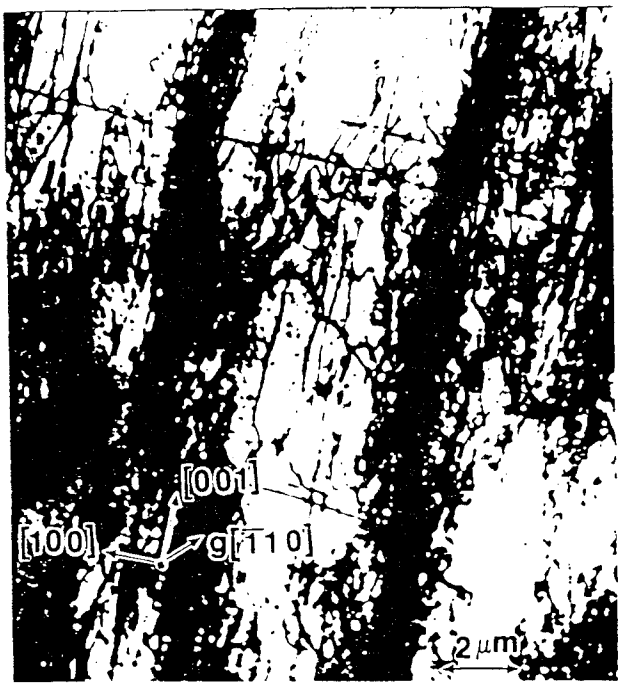

Figure 3. Bright field micrograph showing deformation structure of Ni-50Al.

Electron microscopy observation for the Ni-rich Ni-48Al and the Ni-poor Ni-52Al alloys revealed similar types and configurations of dislocations. However, consistent with the observed shift in slip plane, these off-stoichiometric alloys showed an increased density of <001> dislocations slipping on the {100} slip planes.

The deformed CoAl samples were sectioned parallel to the [010] slip plane in the same manner as the NiAl materials. The resulting observations for the stoichiometric Co-50Al summarized in Figure 4. Dislocations, many in the form of elongated loops, are found to lie within the plane of the foil and are characterized by a general line direction of [100]. Additionally, significant numbers of dislocations appear normal to the foil with a line direction of [010]. Contrast analysis reveals the dislocations lying in the foil have Burger's vectors of both [001] and [010]. These dislocations would be edge dislocations slipping on the (010) and (001) slip planes respectively. A small number of screw dislocations with Burger's vector of [001] have also been observed in the plane of the foil. The dislocations lying normal to the plane of the foil are a mixture of [010] screw dislocations, corresponding with slip on the (001) plane, and a small number of [001] edge dislocations, presumably slipping or climbing on the (100) plane. For the conditions of [011] deformation at 673 K, only these <001> dislocations were observed. However, it should be noted that <001>, <110>, and <111> dislocations have recently been observed in CoAl deformed at higher temperatures using a <123> orientation [27].

Analysis of the Co-52Al (fig. 5) revealed the same operative dislocations as in the stoichiometric alloy. Again, only [100] and [001] screw and edge dislocations were present in the deformed structure. Unfortunately, due to the extreme brittleness of the Co-48Al it has not been possible to successfully prepare a thin foil. This difficulty is consistent with the increased hardness and limited slip lines observed in this alloy.

The results presented here indicate that the deformation of both NiAl and CoAl alloys

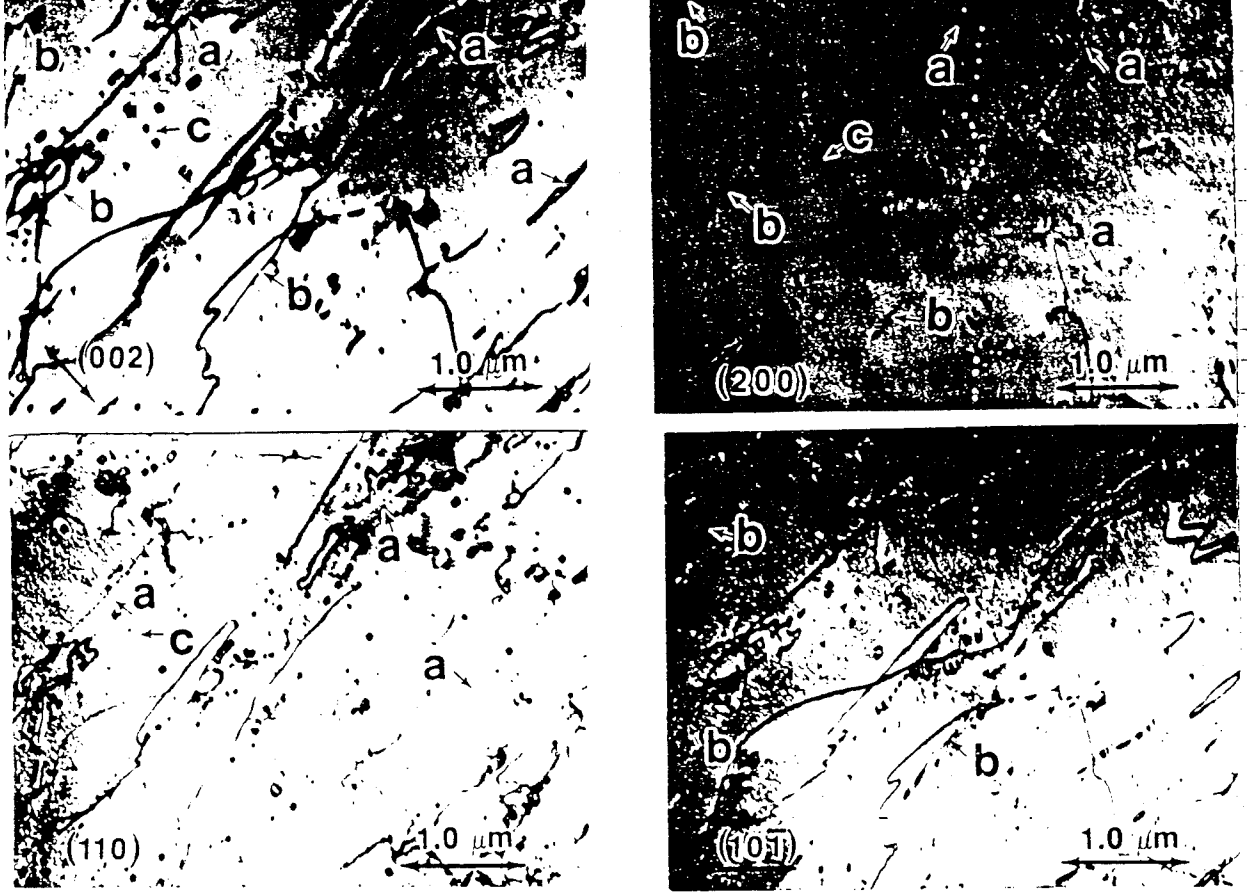

Figure 4. Bright field micrographs illustrating the deformation structure observed in stoichiometric Co-50Al.

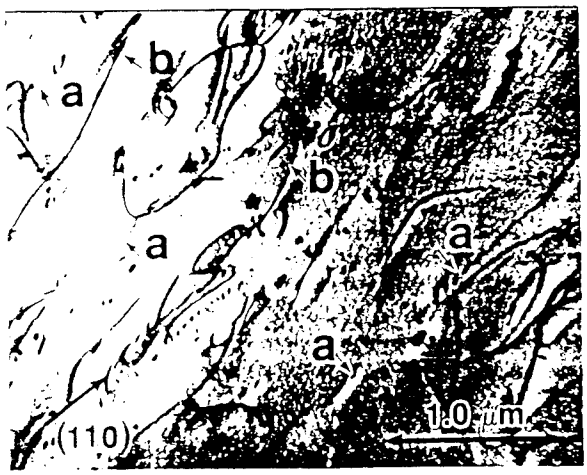

Figure 5. Bright field micrograph showing the dislocation structure in deformed Co-52Al.

deformed at 673 K occurs predominantly by the slip of <001> dislocations. With the exception of stoichiometric Ni-50Al, the dominant slip plane is {100} for these <110> oriented single crystals. Thus it appears that both the CoAl and NiAl alloys are deforming by essentially the same slip mechanisms. In order to rationalize the much greater strength and hardness of CoAl, it must be assumed that the <001> dislocations are fundamentally much harder to move. That is, they have a greater critical resolved shear stress. This occurs although NiAl and CoAl have the same crystal structure and almost identical lattice parameters, and many of their physical properties, such as melting temperature are similar. It is likely that the differences in dislocation slip behavior result from subtle differences in the dislocation core structures in these materials. Recently [28], we have shown changes in the core structure of <001> dislocations as a function of stoichiometry for B2 NiAl alloys. These differences have been related to changes in strength and hardness with changes in stoichiometry [28]. Currently, the structure of the <001> dislocation cores in CoAl are being examined to determine what role this structure plays in controlling the mechanical properties of this class of alloys.

CONCLUSIONS

The deformation behavior of B2 CoAl and NiAl single crystals has been examined as a function of alloy stoichiometry at 673 K using a <110> crystal orientation. Deformation in NiAl was characterized by <001> slip on both {100} and {110} slip planes. A shift in slip plane from predominantly {110} for stoichiometric Ni-50Al to predominantly {100} for off stoichiometric Ni-48Al and Ni-52Al was observed. Although the CoAl alloys were more brittle than the NiAl alloys, the CoAl materials also exhibited <001> slip. The observed slip plane for all of the CoAl alloys was {100} regardless of alloy stoichiometry. In general, a decrease in slip, corresponding to increased strength, was observed for deviations in chemistry form stoichiometry.

ACKNOWLEDGEMENTS

This work was supported by the Office of Naval Research, through grant #N00014-90-J-1910, Dr. G. Yoder contract monitor. Single Crystals of NiAl and CoAl were provided by R. Mahapatra at the Naval Air Development Center, Warminster, PA. Additional Single Crystals of NiAl were provided by Dr. R. Darolia, GE Aircraft Engines, Cincimmati, OH.

REFERENCES

1) R. Darolia, J. of Mat. Sci., **43**, 44 (1991).
2) A.J. Bradley and A. Taylor, Proc. Roy. Soc., **A159**, 56 (1937).
3) A.J. Bradley and G.D. Seager, J. Inst. Metals, **64**, 81 (1939).
4) J.H. Westbrook, J. Electro. Chem. Soc., **103**, 54 (1956).
5) R.L. Fleisher, GE Research and Development Center Alloys Properties Lab., 92CRD181 (1992); J. Mat. Res., in press.
6) A. Ball and R.E. Smallman, Acta Met., **14**, 1349 (1966).
7) R.T. Pascoe and C.W.A. Newey, Met. Sci. J., **2**, 138 (1968).
8) L.A. Hocking, P.R. Strutt, and R.A. Dodd, J. of Inst. Met., **99**, 98 (1971).
9) J.D. Whittenberger, Mat. Sci. and Eng., **73**, 87 (1985); ibid **85**, 91 (1987).
10) J.D. Whittenberger, private communication.
11) R.J. Wasilewski, S.R. Butler and J.E. Hanlon, Trans. Metal. Soc. AIME, **237**, 1357 (1967).
12) N.J. Zaluzec and H.L. Fraser, Script Met. Mat., 8, 1049 (1974).
13) C.W. Marshal and J.O. Brittain, Met. Trans., 7A, 1013 (1976).
14) A. Lasalmonie, J. Mat. Sci., **17**, 2419 (1982).
15) J. Baker and E.M. Schulson, Met. Trans., **15A**, 1129 (1984).
16) P.R. Munroe and I. Baker, Scripta Met. Mat., 23, 495 (1989).
17) M.G. Mendiratand and C.C. Law, J. Mat. Sci., 22, 607 (1987).
18) C.R. Feng and K. Sadananda, Scripta Met. Mat., 24, 2107 (1990).
19) P.R. Munroe and I. Baker, Acta Met. Mat., 39, 1011 (1991).
20) N.H. Lorretto and R.J. Wasilewski, Phil. Mag., 23, 1311 (1971).
21) D.B. Miracle, Acta Met., 39, 1457 (1991).
22) M. Dollar, S. Dymek, S.J. Hwang, and P. Nash, Scripta Met. Mat., 26, 29 (1992).
23) W.D. Nix COSAM Prog. Overview, NASA TM-53006, 183 (1982).
24) D.L. Yaney, A.R. Pelton and W.D. Nix, J. Mat. Sci., **21**, 2083 (1986).
25) D.L. Yaney and W.D. Nix, J. May. Sci., **23**, 3088 (1988).
26) C. J. Drelles, M.S. Thesis, Mich. Tech. Univ., (1985).
27) Y. Zhang and M.A. Crimp, in prep.
28) S.C. Tonn, Y. Zhang and M.A. Crimp, submitted to Mat. Sci. and Eng.

Processing, Properties and Applications of Iron Aluminide Intermetallics, J. Schneibel and M.A. Crimp eds., TMS Proceedings, Warrendale PA., 241 (1994).

STRUCTURAL STUDIES OF <100>{001} EDGE DISLOCATION CORES IN B2 Fe-Al ALLOYS

D. Sharrott, Y. Zhang and M.A. Crimp

Department of Materials Science and Mechanics
Michigan State University
East Lansing, Michigan 48824-1226

Abstract

Stoichiometric Fe-50Al and iron rich Fe-40Al B2 ordered intermetallic single crystals, oriented near (001), have been compressed to approximately 5% plastic strain at 873 K. Conventional transmission electron microscopy revealed <100> edge dislocations with <001> line directions. High resolution electron microscopy was used to image the details of the core structure of these dislocations. Fe-40Al <001>{100} edge dislocation cores were found to be compact with little or no evidence of core spreading. <001>{100} cores in Fe-50Al were found in a number of configurations, including glide dissociation in the slip plane and climb dissociation normal to the slip plane. Comparison with theoretical stuctures revealed significant differences in model and experimentally observed structures.

Introduction

Dislocation structures have been studied extensively in B2 alloys in order to better understand the ductility and fracture problems associated with this class of materials. In particular, NiAl has received the focus of many of these studies. However, FeAl and CoAl continue to receive considerable attention as well.

The predominant slip modes in NiAl [1-6] are <100>{001} and <100>{011}, in both polycrystalline and single crystal specimens. <111> slip can be activated at low temperatures and/or by orienting single crystals to hard orientations (near [001]) [6-11]. In NiAl, <111> dislocations have also been activated by alloying additions [12,13]. However, improvements in the properties of NiAl have not been realized by the activation of <111> slip. On the other hand, the toughness of NiAl has been improved through heat treatment control and pre-strain pressure effects [14-19]. At this point it is not entirely clear what mechanisms are involved with this improvement in properties.

Deformed CoAl has been found to display predominately <100> dislocations over a wide range of temperatures [20-22]. However, some <111> and <110> dislocations have also been observed [22]. Despite the various types of dislocations observed in CoAl, this alloy suffers from extreme brittleness, even at relatively high temperatures.

In contrast with NiAl and CoAl, B2 FeAl deforms predominantly by <111> slip at low to moderate temperatures [23,24]. While this <111> slip in FeAl does not lead to significant ductility in stoichiometric alloys, iron rich compositions display substantial ductilities and reasonable toughnesses [25-27]. This appears to be directly related to a decrease in the critical resolved shear stress of <111> slip with increasing iron rich deviations from stoichiometry [28]. At moderate temperatures, a transition from <111> to <100> slip has been characterized for both single [23,24] and polycrystalline [29] samples. Materials deformed above this slip transition display very high ductilities [26]. In addition to <100> slip, there have been limited observations of <110> slip in these materials [30].

It is well known that the deformation behavior of bcc metals has been related to the core structure of the <111> screw dislocations as determined by computer simulation techniques [31]. The dislocation core structures in B2 alloys have also been studied by atomistic models in an effort to relate the core structure to slip behavior [32-37]. Recent advances in high resolution electron microscopy (HREM) have made it possible to experimentally image select dislocation core structures, thus allowing comparison with model structures. This is leading not only to a better understanding of dislocation cores and their relationship to mechanical behavior, but also provides critical analyses for current computer models. These comparisons enable improvements to be made in modeling procedures and interatomic potentials.

In the present study, the core structures of dislocations in FeAl are examined at two stoichiometries. While the core structure of <111> screw dislocations is of keen interest in FeAl and other B2 materials, limitations in the HREM technique make these cores unsuitable for study. Thus, <100> dislocations have been introduced during high temperature deformation for examination. An advantage of choosing <100> dislocations is that it allows comparison with <100> core structures observed in NiAl and CoAl, which are presently being examined by our group. These comparisons may lead to a better understanding of dislocation slip and mechanical response of the various B2 aluminides.

Experimental Procedure

Single crystal compression samples with dimensions 9mm x 3mm x 3mm and nominal compositions of Fe-50at%Al and Fe-40at%Al were cut from bulk specimens using a high speed wafering saw. Bulk specimen dimensions limited the selection of deformation axes to

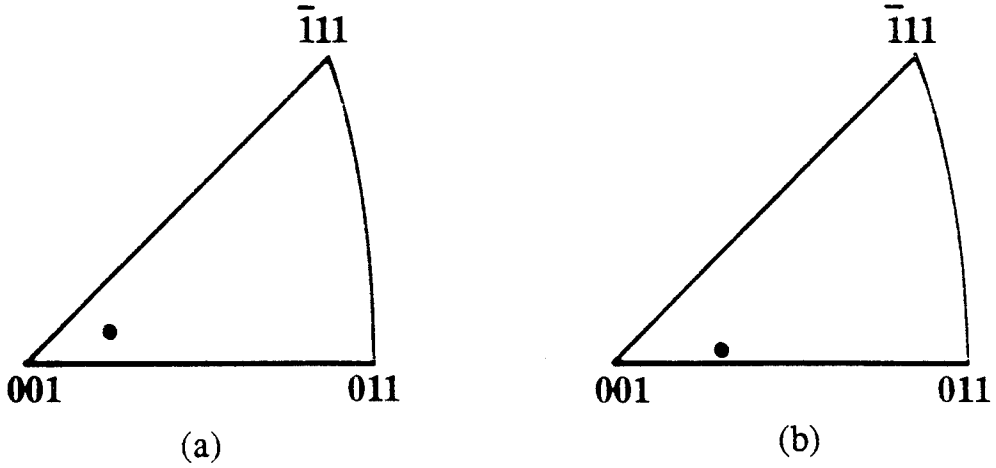

Fig. 1. Standard Stereographic triangles showing single crystal compression axes for (a) Fe-40Al and (b) Fe-50Al.

orientations near [001] as shown in fig. 1. In order to encourage the activation of <100> slip, deformation was carried out at 873 K (~0.67Tm). Compression was carried out in vacuum at a nominal strain rate of 2.5×10^{-4}/sec to approximately 5% plastic strain. Specimens were furnace cooled following release of the deformation load. Slip lines were observed using optical microscopy with polarized light. Slip planes were determined by standard two face slip trace analysis.

Thin foils for conventional TEM were prepared by sectioning parallel to the observed slip plane while those for HREM were sectioned normal to the [010] direction. Foils were electro-polished in a solution of 1 part HNO_3 to 2 parts methanol at -20°C with a voltage of 12 V. Conventional diffraction contrast TEM was performed in a Hitachi H-800 at 200 kV, while HREM was performed at 350 kV in a JEOL-4000EX.

HREM image simulations were based on a theoretical core structure determined by Vailhe and Farkas [38] using the embedded atom method. The image simulations were performed using the EMS software package [39].

Results and Discussion

Characterization of slip

Deformation of the orientated single crystals resulted in well defined slip lines, an example of which is given in fig. 2. The slip is characterized by planer slip with a small amount of waviness indicative of cross slip. Slip trace analysis of both stoichiometric Fe-50Al and iron rich Fe-40Al, somewhat surprisingly, found the slip planes to be {110}.

Sections cut parallel to this observed {110} slip plane were prepared for conventional transmission electron microscopy and revealed substructures made up predominantly of straight dislocation segments lying roughly 90° to one another. Trace analysis determined the two general line directions to be [100] and [010]. Diffraction contrast analysis was used to characterize the Burger's vectors of these dislocations with an example given for Fe-40Al in fig. 3. Due to the elastic anisotropy of FeAl, it can be difficult to get complete invisibility of dislocations under the conditions of $\mathbf{g} \cdot \mathbf{b} = 0$. Ideally, a complete analysis can be performed using computer simulations following the method of Head et. al. [40]. However, if the condition $\mathbf{g} \cdot \mathbf{b} \times \mathbf{u} = 0$ is used in conjunction with the $\mathbf{g} \cdot \mathbf{b} = 0$ criteria, a reasonable analysis can be performed. In fig. 3 the dislocation labeled (a) has line segments in the [100] and [010] directions. The

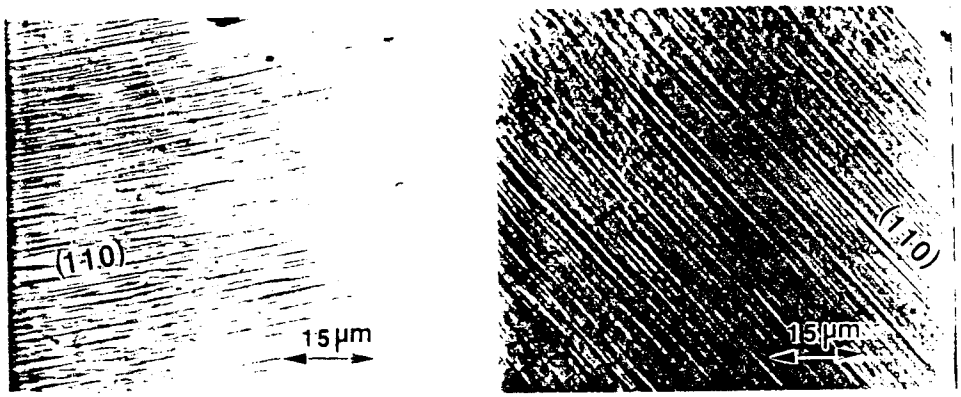

Fig. 2. Optical micrographs showing slip bands on two faces of a Fe-50Al single crystal deformed at 873 K. {110} slip plane traces are indicated.

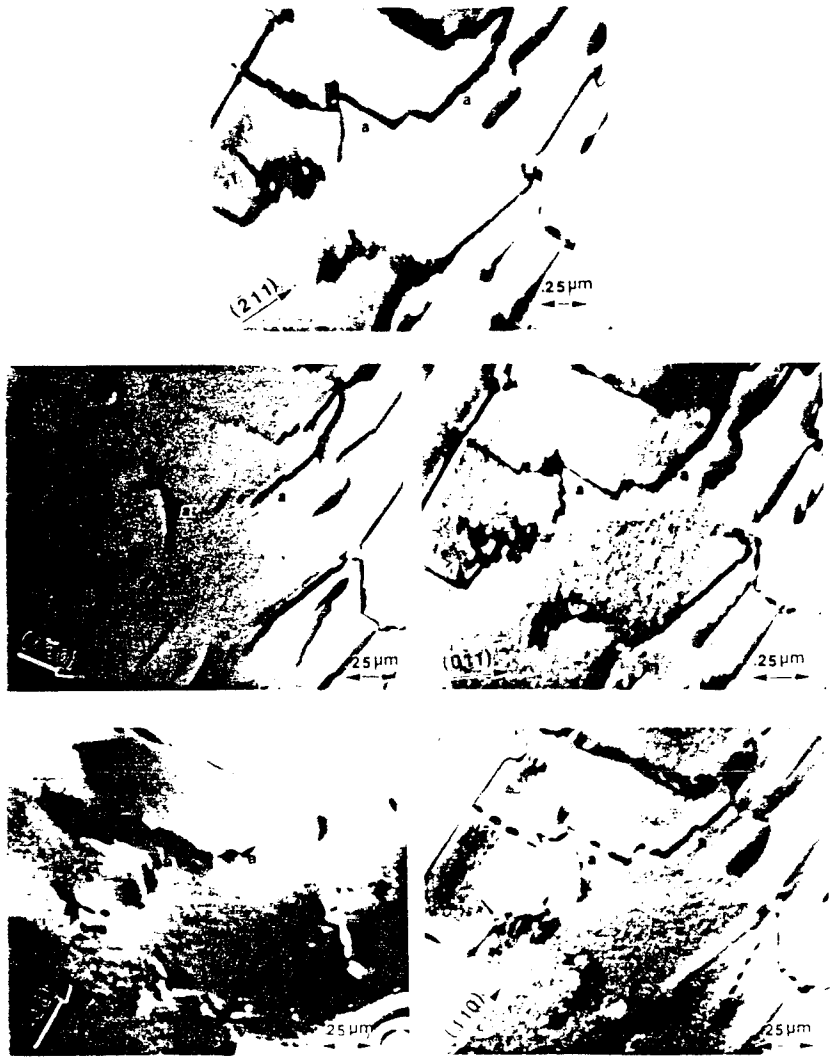

Fig. 3. Conventional diffraction contrast images of the dislocation structure of Fe-40Al deformed at 873 K. Note that the dislocation labeled (a) has a Burger's vector of [001] and line directions of [100] and [010] indicating this is a prismatic dislocation.

segment in the [010] direction is well out of contrast for $\mathbf{g}=(0\bar{2}0)$ while the segment in the [100] direction is out of contrast for $\mathbf{g}=(200)$. The segments which are not parallel with the operative g-vectors display weak contrast for these reflections. Applying the $\mathbf{g}\cdot\mathbf{b}=0$ and $\mathbf{g}\cdot\mathbf{b}\times\mathbf{u}=0$ criteria to these observations leads to the conclusion that $\mathbf{b}=[001]$. Other dislocations in this figure show

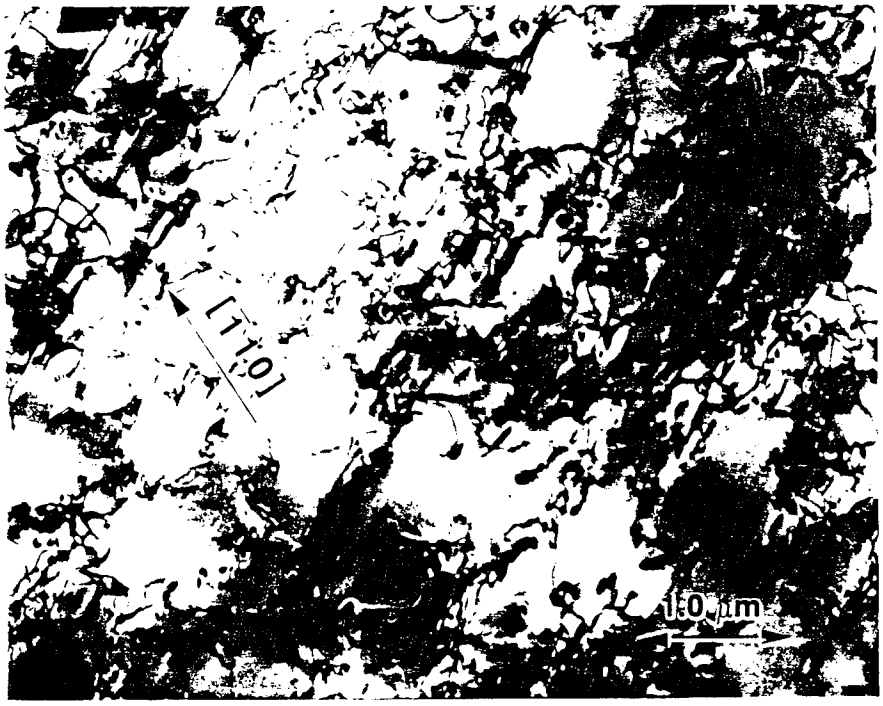

Fig. 4. Diffraction contrast image displaying the deformation strucuture of Fe-50Al compressed at 873 K.

similar results. It should be noted that since the line directions of the segments of dislocation (a) are [100] and [010], the [001] Burger's vector of this dislocation lies normal to the plane of the dislocation. This result appears to contradict the results of the slip trace analysis, which found {110} to be the operative slip plane. However, some dislocation rearrangement may have occurred during the furnace cooling following deformation. Prismatic loops and dislocations, with **b**=<100> lying normal to the slip plane, have been observed in FeAl on a number of occasions [41-43]. Fe-50Al displayed a similar deformation structure to that observed in Fe-40Al, an example of which is shown in fig. 4.

Experimental images of dislocation cores

Since the majority of the dislocations in the deformed materials displayed <100> line directions, thin foils for HREM were prepared by sectioning normal to either the [100] or [010]. This allowed the core structure of the dislocations to be imaged "end on" down a low index zone with lattice spacings greater than the resolution limit of the microscope.

Surprisingly, high resolution electron microscopy of Fe-40Al revealed not only **b**=<001> dislocations, but also **b**=<110> dislocations. The present study will concentrate on the <001> dislocations while the <110> dislocations will be discussed elsewhere [44]. Figure 5 shows a HREM image of a **b**=[001](100) edge dislocation. This image and all other HREM images presented in this paper are "white atom" images with the lighter contrast areas signifying the approximate atom positions. Although the dislocations may not be moving by slip, for discussion purposes the slip plane will be considered to be the plane defined by **bxu**. Accompanying this experimental image are digitally scanned and compressed images which allow the displacements in various directions and the termination of atomic planes to be more easily seen. These images give an illusion of the image being veiwed down a given direction at an inclined angle. The core structure shown in fig. 5 can be characterized by two distinct {220} half planes which terminate near the same point in the dislocation core. The approximate locations of these half planes are denoted by the arrows in fig. 5a and can be more clearly seen in figs 5b and 5c. The core is compact, with only slight spreading in the (100) slip plane (fig.

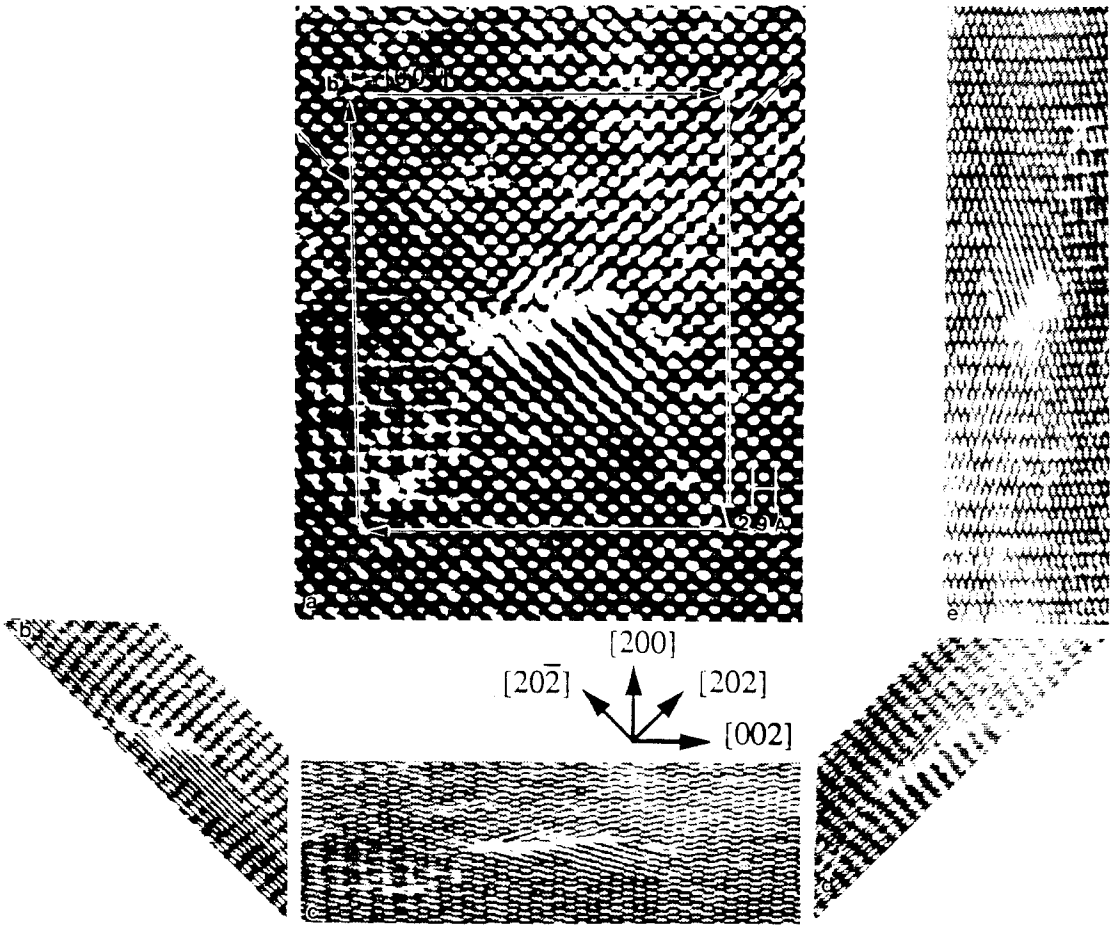

Fig. 5. (a) HREM image of a **b**=[001](100) dislocation in Fe-40Al. (b-e) Digitally compressed images of (a), corresponding to views down the (b) [202], (c) [200], (d) [20$\bar{2}$] and (e) [002] directions.

5c) and no significant displacements normal to the slip plane (fig. 5e). This structure is similar to the <001>{100} cores observed in Ni-50Al [45,46] and Ni-48Al [46].

A number of different core configurations of [001](100) edge dislocations were observed in Fe-50Al. The first of these is shown in fig. 6 and is similar in configuration to the [001](100) dislocation core observed in Fe-40Al. Again, the core is compact with the characteristic {220} half planes terminating at approximately the same location. However, these terminations actually lie at positions above one another relative to the slip plane. This may be indicative of some climb process having taken place.

An alternative [001](100) Fe-50Al edge dislocation core structure is shown in fig. 7. In this structure, the characteristic {220} half planes terminate approximately 10-12 atom positions from one another in the plane of the [001] Burger's vector. This clear dissociation can be characterized by two separate Burgers vectors, ½[101] and ½[$\bar{1}$01] as illustrated in the figure. Thus, the dissociation might be thought of as:

$$a[001] = a\tfrac{1}{2}[\bar{1}01] + a\tfrac{1}{2}[101] \qquad [1]$$

However, it should be reiterated that HREM can only resolve the edge component of dislocations. This implies one may not rule out the possibility that there may be a screw component in the beam direction ([010] in this figure) which is not resolved. Thus, equation [1] only involves the edge components and can be thought of as:

Fig. 6. HREM image of a [001](100) dislocation core in deformed Fe-50Al. Note how the {220} extra half planes terminate at positions above one another relative to the plane of the Burger's vector.

$$a[001]_e = a/2[\bar{1}01]_e + a/2[101]_e \qquad [2]$$

with the subscript "e" indicating edge components. Since $\frac{1}{2}$<110> dislocations in the B2 structure do not translate the lattice from one atomic position to another, a more likely dissociation may be:

$$a[001] = a/2[\bar{1}11] + APB + a/2[1\bar{1}1] \qquad [3]$$

The ordering of the B2 lattice requires that an antiphase boundary (APB) lie between the $\frac{1}{2}$<111> dislocations. This dissociation scheme is not energetically favorable based on linear elasticity. However, Fourdeux and Lesbats [42] have shown the dissociation of <100> dislocations into two APB coupled $\frac{1}{2}$<111> dislocations to be a mechanism for vacancy annihilation in Fe-42Al.

Figure 8 shows a dipole between two <100> dislocations with their slip planes separated by approximately 10 atomic spacings. This dipole may be the result of slip interaction between these two dislocations, but linear elasticity suggests that the energy minimum between two dipole dislocations occurs when the dislocations lie 45° to each other, relative to the Burger's vector and slip plane. Instead, the experimental image shows the dipole dislocation cores lying approximately 90° to one another. It may be that this dipole formed as the result of vacancy coalescence. It is well known that thermal vacancies in FeAl anneal out into dislocation loops and helices [41,42,47]. Close analysis of the Burger's vector circuits in fig. 8 shows that this dipole is a vacancy/intrinsic dipole and not an extrinsic dipole. This is illustrated by comparison with fig. 9. Thus this dipole core configuration may in fact be a prismatic loop nuclei. It should also be noted that close analysis of each of the individual <001> dislocations in this dipole shows the arrangement of the {220} extra half planes to be somewhat different in the two

Fig. 7. Experimental HREM image of a [001](100) edge dislocation in Fe-50Al. Note how the {220} extra half planes terminate approximately 10-12 atom positions apart on the slip plane possibly indicating a glide dissociation.

dislocations. It is possible that the core structures of these dislocations vary during the climb process.

Comparison of experimental images with model structures

Vailhe and Farkas [38] have recently performed an embedded atom simulation of the core structure of a <001>{100} edge dislocation in stoichiometric Fe-50Al. It is useful to examine how this theoretical structure compares with the experimental images of the core structures imaged in the present work. Figure 10 shows a plot of the atomic positions determined by Vailhe and Farkas, along with a series of simulated HREM images based on this theoretical structure. The theoretical structure displays a compact core with no evidence of significant spreading in the slip plane or any indication of climb. The {200} extra half planes can be seen to terminate within one atomic position of each other.

This theoretical structure is significantly different from the structures observed experimently. In the one experimental image of a compact core in Fe-50Al (fig. 9), some climb dissociation was noted. Of course EAM could not predict such a structure, unless the climb component was introduced in the initial structure. In the experimental image of the core spread on the slip plane shows a significant dissociation of 10-12 atom spacings. This is in contrast with the EAM result. The reasons for these differences are not entirely clear. One possibility is that there is an experimental artifact, such as free surface effects or the presence of a residual stress in the thin foil, causing the dissociation in the slip plane. On the other hand, the experimental results may indicate a problem with the approach to the simulation, such as the choice of the elastic center of the dislocation or the details of the interatomic potentials. Clearly, more work is needed in order to rationalize these differences in theoretical models and experimental images.

Fig. 8. HREM image showing a dipole between two <100> dislocations in Fe-50Al. Note that the two dislocations lie approximately 10 atomic spacings apart in the [100] direction.

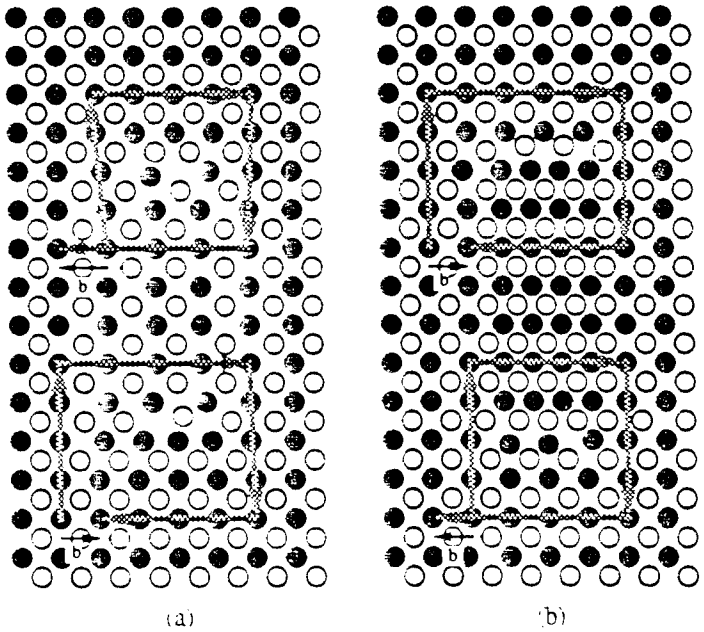

Fig. 9. Schematic illustations of (a) a vacancy dipole like that shown in fig. 9 and (b) a interstitial dipole.

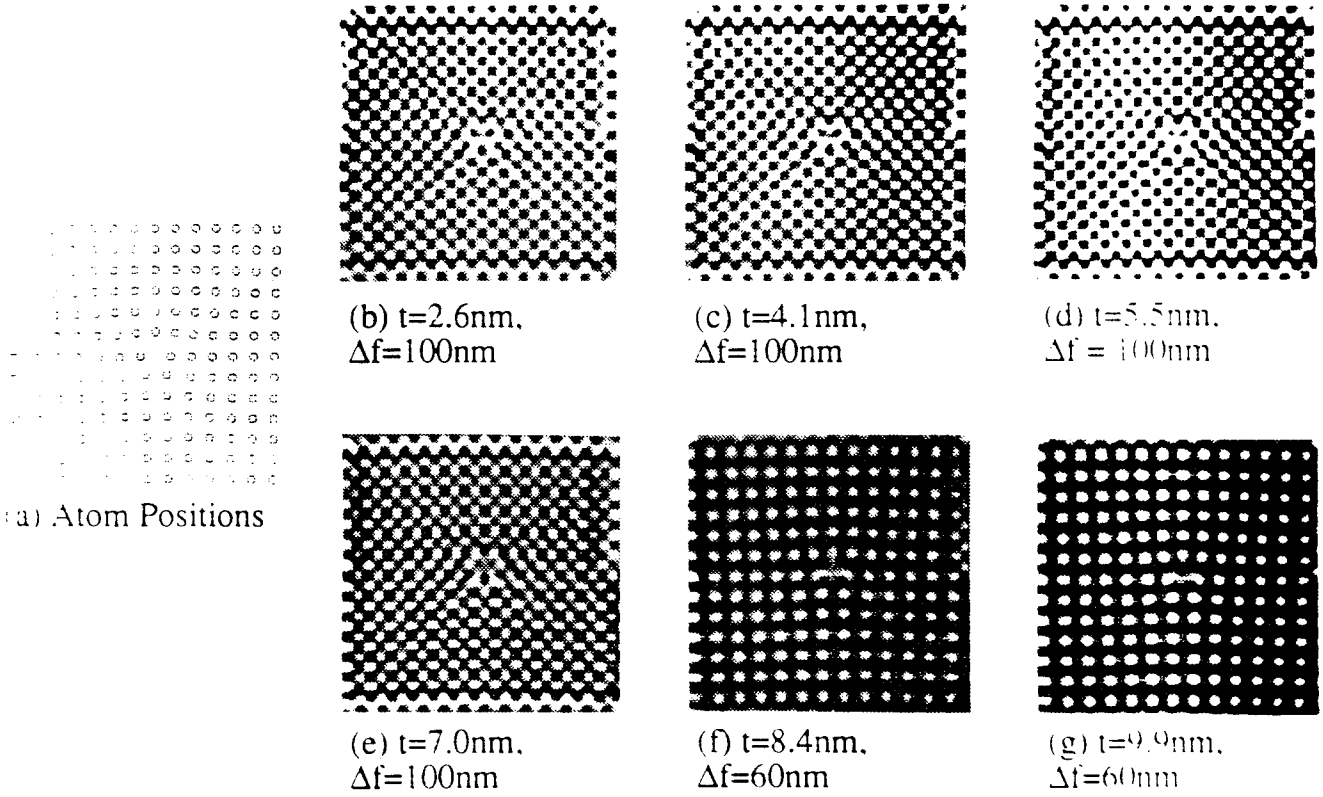

Fig. 10. (a) Atom positions for a <001>{100} edge dislocation as determined by EAM. (b-g) Simulated HREM images based on atom positions shown in (a).

Conclusions

Experimental imaging of <001>{100} edge dislocation core structures in B2 FeAl alloys show a variety of configurations. In Fe-40Al these dislocations appear to have compact cores with only slight spreading in the (100) slip plane. No evidence of climb was observed in this alloy for the <001>{110} dislocations. In Fe-50Al, <001>{100} cores displayed two configurations, one being compact with a small climb dissociaton normal to the slip plane, the other showing dissociation into two ½<111> dislocations separated by approximately 10-12 atom spacings along the slip plane. Additionally, a dipole core which appears to be a prismatic loop nuclei has been observed in Fe-50Al. Comparisons of the experimental images with theoretical structures suggest that significant differences in the structures exist.

Acknowledgements

The authors would like to acknowledge the support of the Office of Naval Research through grant number ALP-90-J-1910, Dr. G. Yoder, Scientific Officer. The authors would also like to thank Mr. C. Vailhe and Dr. D. Farkas of Virginia Polytechnic Institute and State University for providing the results of their EAM calculations and Dr. R. Neobe of NASA LRC and Dr. S. Hartfield for providing the Fe-40Al single crystals. The HREM was performed at the University of Michigan Electron Microbeam Analysis Laboratory, Dr. J.F. Mansfield Director.

References

1. A. Ball and R.E. Samllman, Acta Met., **14** 1349 (1966).

2. C.H. Lloyd and M.H. Loretto, Phys. Stat. Sol., **39** 163 (1970).

3. R.J. Wasilewski, S.R. Butler and J.E. Hanlon, Trans. AIME **239** 1357 (1967).

4. J. Bevk, R.A. Dodd and P.R. Strutt, Met. Trans., **4** 159 (1973).

5. H.L. Fraser, R.E. Smallman and M.H. Loretto, Phil. Mag., **28** 651 (1973).

6. J.T. Kim and R. Gibala, MRS Proceedings vol. 213, L.A. Johnson, D.P. Pope and J.O. Stiegler eds., **213** 261 (1991).

7. M.H. Loretto and R.J. Wasilewshi, Phil Mag., **23** 1331 (1971).

8. R.G. Campany, M.H. Loretto and R.E. Smallman, J. Microscopy, **98** 174 (1967).

9. P. Veyessiere and R. Noebe, Phil. Mag. A., **65** 1 (1992).

10. R.D. Field, D.F. Lahrman and R. Darolia, Acta Met. et Mat., **39** 2951 (1991).

11. Y.Q. Sun and G. Taylor, Proc. 3rd Japan Int. SAMPE Sym. on Intermetallic Compounds for High Temp. Structural Applications, M. Yamaguchi and H. Fukutomi eds., 1230 (1993).

12. C.C. Law and M.J. Blackburn, Final Technical Report AFWAL-TR-87-4102 (1987).

13. D.B. Miracle, S. Russell and C.C. Law, MRS Proceedings vol. 133, C.T. Liu, A.I Taub, N.S. Stoloff and C.C. Kock eds., **133** 225 (1989).

14. J.E. Hack, J.M. Brezski, R. Darolia, Scripta Met. et Mat. **27** 1259 (1992).

15. J.E. Hack, J.M. Brezski, R. Darolia and R.D. Field, MRS Proceedings vol. 288, I.Baker, R. Darolia, J.D. Whittenberger and M.H. Yoo eds., **288** 1197 (1993)

16. J.M. Brzeski and J.E. Hack, Mat. Sci. and Eng., **A170** 11 (1993).

17. R.W.Margevicius and J.J. Lewandowski, Scripta Met. et Mat., **25** 2017 (1993).

18. R.W. Margevicius, J.J. Lewandowski and I. Locci, Scripta Met. et Mat., 26 1722 (1992).

19. R.W. Margevicius and J.J. Lewandowski, Acta Met. et Mat., **41** 485 (1992).

20. D.L. Yaney and W.D. Nix, J. Mat. Sci., **21** 2083 (1986).

21. D.L. Yaney and W.D. Nix, J. Mat Sci., **23** 3088 (1988).

22. Y. Zhang and M.A. Crimp, Unpublished Research.

23. Y. Umakoshi and M. Yamaguchi, Phil. Mag. A, **41** 573 (1980).

24. Y. Umakoshi and M. Yamaguchi, Phil. Mag. A, **44** 711 (1981).

25. M.A. Crimp, K. Vedula and D.J. Gaydosh, MRS Proceedings vol. 81, N.S. Stoloff, C.C. Koch, C.T. Liu and O. Izumi eds., **81** 499 (1987).

26. M.A. Crimp and K.M. Vedula, Mat. Sci. and Eng., **A165** 29 (1993).

27. C.T. Liu, E.H. Lee and C.G. McKamey, Scripta Met., **23** 875 (1989).

28. M.A. Crimp and K. Vedula, Phil. Mag. A, **63A** 559 (1991).

29. M.G. Mendiratta, H-M. Kim and H.A. Lipsitt, Met. Trans. A, **15A** 395 (1984).

30. J.R. Stephens, MRS Proceedings vol. 39, C.C. Koch, C.T. Liu and N.S. Stoloff eds., **39** 381 (1985).

31. J.W. Christian, Met. Trans A, **14A** 1237 (1983).

32. M. Yamaguchi and Y. Umakoshi, Scripta Met., **9** 637 (1975).

33. S. Takeuchi, Phil. Mag. A, **41A** 541 (1980).

34. M. Yamaguchi and Y. Umakoshi, Phys. Stat. Sol. (a), **31** 101 (1975).

35. K. Benhaddane and P. Beauchamp, Phys. Stat. Sol. (a), **98** 195 (1986).

36. M.J. Mills, M.S. Daw, S.M. Foiles and D.B. Miracle, MRS Proceedings vol 288, I. Baker, R. Darolia, J.D. Whittenberger and M.H. Yoo eds., **288** 257 (1993).

37. R. Pasianot, D. Farkas and E.J. Savino, J. Phys. III, **1** 997 (1991).

38. C. Vailhe and D. Farkas, Private Communication.

39. P. Stadelmann, Ultramicroscopy, **21** 131 (1987).

40. A.K. Head, P. Humble, L.M. Clarebrough, A.J. Morton and C.T. Forwood, Defects in Crystalline Solids vol. 7, S. Amelinckx, R. Gevers and J. Nihoul eds., North-Holland (1973).

41. N. Junqua, J.C. Desoyer and J. Grilhe, Acta Met., **30** 395 (1982).

42. A. Fourdeux and P. Lesbats, Phil. Mag., A, **45** 81 (1982).

43. M.A. Crimp, Ph.D. Dissertation, Case Western Reserve Univ., (1987).

44. D.S. Sharrott, Y. Zhang and M.A. Crimp, to be submitted to Mat. Sci. and Eng.

45. M.J. Mills and D.B. Miracle, Acta Met. Mater., **41** 85 (1993).

46. M.A. Crimp, S.C. Tonn and Y. Zhang, Mat. Sci. and Eng., **A170** 95 (1993).

47. N. Junqua, J.C. Desoyer and P. Moine, Phys. Stat. Sol. (a), **18** 387 (1973).

typographical corrections will be accepted at this stage

256 Banbury Road
Oxford OX2 7DH
U.K.

EDITOR

9 .....PAGES

MSE 5208

ELSEVIER

Materials Science and Engineering A000 (1994) 000–000

MATERIALS SCIENCE & ENGINEERING A

High-resolution electron microscopy (HREM) examination of dislocation core structure in B2 Fe–Al single crystals

D. Sharrott, M.A. Crimp

Department of Materials Science and Mechanics, Michigan State University, East Lansing, MI 48824-1226, USA

Abstract

Stoichiometric Fe–50at.%Al and iron-rich Fe–40at.%Al single crystals oriented near {001} have been deformed in compression at 873 K to approximately 5% plastic strain. Conventional diffraction contrast transmission electron microscopy (TEM) has been used to characterize the dislocation structures in these materials. The observed dislocations are predominantly ⟨001⟩{001} prismatic edge dislocations, with a small number of ⟨111⟩ screw dislocations. The atomic level details of the core structures of these dislocations have been examined using phase contrast TEM and high-resolution electron microscopy (HREM). Dislocations with both glide and climb dissociated core structures have been observed. The implications of these structures on the mechanical behavior (at both low and elevated temperatures) are discussed.

Keywords: HREM; Dislocation; Iron; Aluminium; Crystals

1. Introduction

Dislocation structures have been studied extensively in the B2 aluminides (FeAl, NiAl and CoAl) in order to gain a better insight into the ductility and fracture problems associated with this class of materials. The slip characteristics of FeAl are significantly different from those found in NiAl and CoAl, due to the fact that B2 FeAl deforms predominantly by ⟨111⟩-type slip at low to moderate temperatures [1,2]. Although ⟨111⟩ slip does not lead to substantial ductility for stoichiometric B2 FeAl at ambient temperatures, increased ductility and toughness are observed for alloys with increasingly iron-rich deviation from stoichiometry [3–5]. There appears to be a direct relationship between the decrease in the critical resolved shear stress for ⟨111⟩ slip and increasing iron content from the stoichiometric composition [6]. At moderately elevated temperatures, a transition in slip from ⟨111⟩ to ⟨100⟩ has been observed in single-crystal [2] and polycrystalline [7] FeAl. This transition temperature (around $0.4–0.5T_m$) has been found to increase with increasing aluminum content for single crystals [2], while decreasing with increasing aluminum content for polycrystalline samples [7]. Stoichiometric B2 FeAl deformed at temperatures above this transition temperature has been found to display very high ductility [8]. There have been limited observations of ⟨110⟩ dislocations in this material [9].

An interesting complication to understanding the behavior of this material has to do with the effect of the cooling rate on the mechanical properties of FeAl. It is well established that there is a strong relationship between the vacancy concentration and thermal treatment of this material. Correspondingly, both elevated temperature and quenching rate tests have shown that thermal treatment can have a profound effect on the mechanical behavior of FeAl.

The first studies of quenched-in vacancies in FeAl were carried out using resistivity, dilatometry and field ion microscopy [10–13]. These studies found quenched-in vacancy concentrations as high as 1.4×10^{-2} and 2.2×10^{-2} as quenched from 1050 °C ($0.86T_m$) for Fe–46at.%Al and Fe–51at.%Al respectively. Typical metals have vacancy concentrations on the order of 10^{-3}–10^{-4} near their melting points [14]. In situ electron microscopy observations have shown that these excess vacancies anneal out into dislocation loops, helices, super-structure dislocation loops and paired helices bound by antiphase boundaries (APBs)

0921-5107/94/$7.00 © 1994 – Elsevier Science S.A. All rights reserved

[15–17]. These vacancy products appear to nucleate on inclusions and pre-existing dislocations. The resultant dislocation loops and helices have both ⟨100⟩ and ⟨111⟩ Burgers vectors. The ⟨111⟩ helices are observed as both perfect ⟨111⟩ helices and APB coupled $\frac{1}{2}\langle 111\rangle$ helices [15,16]. Furthermore, dissociation of ⟨100⟩ dislocations into APB coupled $\frac{1}{2}\langle 111\rangle$ dislocations is commonly observed. In all of these studies, vacancy-related mechanisms are believed to be directly responsible for the various dislocation reactions. Furthermore, Fordeux and Lesbats [16] concluded that homogeneous vacancy coalescence into voids does not occur in B2 FeAl due to the strong tendency for ordering in this alloy [14].

The effect of thermal history on the mechanical behavior of B2 FeAl was first realized by Rieu and Goux [10] and Weber et al. [18] who attributed increases in hardness following quenching to increases in the number of retained vacancies. This effect is reflected in changes in the tensile behavior showing large increases in yield strength with corresponding decreases in ductility [4,19]. Hardness tests carried out over a wide range of compositions and following a variety of cooling rates and annealing treatments have reinforced these findings [20,21]. Studies on single crystals have related this increase in strength to an increase in the CRSS for ⟨111⟩ slip [6].

Despite the considerable attention that vacancy hardening in B2 FeAl alloys has received, the exact strengthening mechanisms remain unclear. It has been hypothesized that vacancies may act as point defect strengtheners (pin dislocations), may change the degree of long-range order (APB energy) and/or vacancies may coalesce to form material strengthening jogs on existing dislocations [6,15,16]. However, no conclusive evidence for the exact mechanisms has been presented thus far.

The purpose of this paper is to present the results of high- resolution electron microscopy (HREM) studies of the core structures of dislocations in deformed B2 FeAl. This study is part of a larger program examining the differences in the dislocation core structure of the B2 aluminides. The results presented here show that a variety of dislocation core configurations may occur in FeAl. Some configurations may be related to dislocation core–vacancy interaction which may help to explain some aspects of vacancy hardening in these alloys.

2. Experimental details

Bulk single-crystal samples of nominally Fe–50at.%Al and Fe–40at.%Al were fashioned into 9 mm × 3 mm × 3 mm compression specimens using a high speed diamond wafering saw. This 3:1 height to width ratio was used to promote homogeneous deformation. The compression specimens received a 24 h annealing treatment at 1273 K under vacuum, followed by step cooling at a rate of 100 K h^{-1} down to 500 K, then furnace cooling. Specimens were hand polished starting with 600 grit SiC paper and finishing with 0.1 μm diamond paste. Back reflection Laue X-ray studies determined all of the compression axes to be within 15° of [001]. Compression was carried out in vacuum at 873 K (approximately $0.67T_m$) in order to promote ⟨100⟩ slip. Tests were performed at a nominal strain rate of 2.4×10^{-4} s^{-1} to a plastic strain of approximately 5%. The specimens were furnace cooled following release of the deformation load.

Following compression, slip lines were observed using polarized light optical microscopy. The active slip planes were determined by standard two face analysis. Specimens for conventional diffraction contrast transmission electron microscopy (TEM) were sectioned parallel to {001} and {101} planes, while specimens for HREM were sectioned normal to the [100] or [010] directions. The sections were mechanically ground using 600 grit paper to approximately 150 μm. Final thinning was carried out using a twin jet electropolisher with an electrolyte of 30% HNO_3 in methanol at −20 °C and a voltage of 12 V. Conventional TEM was carried out at 200 kV using a Hitachi H-800, while HREM was performed at 350 kV in a JEOL 4000EX.

3. Results

3.1. Slip characterization

Optical microscopy of the deformed single crystals revealed well-defined slip lines as illustrated in Fig. 1. The slip was generally planar in nature with some waviness, indicative of cross slip. Two face slip trace analysis revealed the active slip plane to be {110} in both stoichiometric Fe–50at.%Al and iron-rich Fe–40at.%Al.

Characterization of the deformation substructures was carried out using conventional TEM performed on sections cut parallel to the active {110} planes. The majority of the dislocations had straight line segments with sharp jogs. The straight segments lay in two primary orientations, roughly perpendicular to one another. Trace analysis revealed these primary directions to be ⟨100⟩ and [010]. Due to the elastic anisotropy of Fe–Al, Burgers vector analysis can be difficult to perform as $\boldsymbol{g}\cdot\boldsymbol{b}=0$ does not always lead to complete invisibility. However, if the $\boldsymbol{g}\cdot\boldsymbol{b}\times\boldsymbol{u}=0$ criterion is used in conjunction with the $\boldsymbol{g}\cdot\boldsymbol{b}=0$ criterion, a thorough

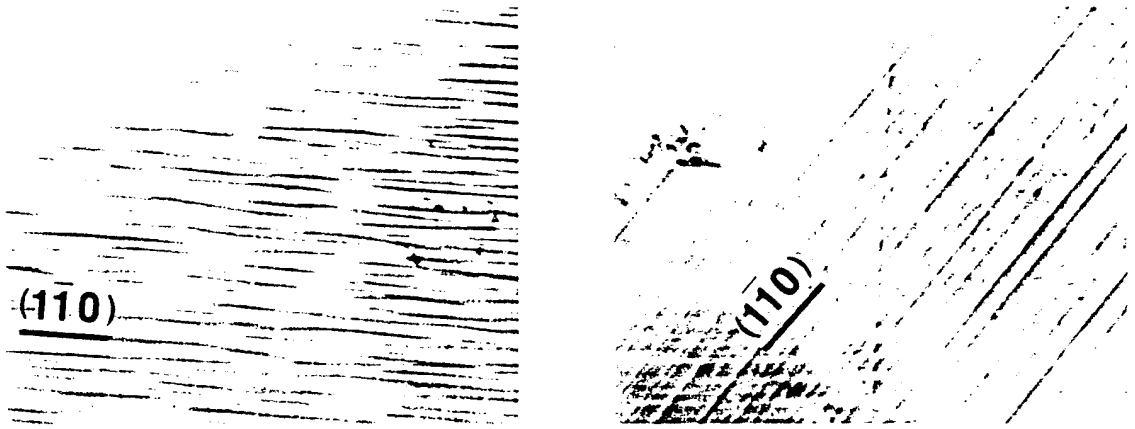

Fig. 1. Optical micrographs showing ⟨110⟩ slip plane traces on two faces of an Fe–40at.%Al single crystal deformed at 873 K.

analysis can usually be carried out. An example of this analysis for deformed Fe–40at.%Al is illustrated in Fig. 2. The dislocation labeled (a) in this figure is typical of the dislocations observed in this material. This dislocation has segments with line directions [100] and [010]. The [100] segments are well out of contrast for $g=\langle 200\rangle$, while the [010] segments display significant contrast for this reflection. Conversely, the [010] segments are out of contrast for $g=\langle 0\bar{2}0\rangle$, while the [100] segments show residual contrast. Applying the $g\cdot b=0$ and $g\cdot b\times u=0$ criteria leads to the conclusion that the Burgers vector of this dislocation is $b=[001]$. Similar analyses show that the majority of dislocations in both Fe–40at.%Al and Fe–50at.%Al have $b=[001]$. It should be noted that the plane of the dislocation (as defined by the line directions of the segments) is (001). This is contrary to the results of the slip trace analysis, which indicated that {110} was the active slip plane. However, as the Burgers vectors of the dislocations are normal to the plane of the dislocations, the dislocations are in prismatic configurations and this finding would not be expected to be consistent with the observed slip lines. It should be noted that prismatic dislocations and loops with $b=\langle 100\rangle$ have been observed in FeAl in a number of studies [16,17,22]. In addition to the $b=[001]$ dislocations observed in the deformed materials, a small number of ⟨111⟩ screw dislocations were also found. Fig. 3 shows an analysis of these dislocations in Fe–50at.%Al.

3.2. High resolution electron microscopy

Atomic resolution imaging of dislocation cores using HREM requires that the dislocations be imaged "end on", i.e. the dislocation line direction must be parallel to the electron beam direction. Secondly, the dislocation must have significant atomic displacements normal to the beam direction in order for the core to be imaged. In fact, only the edge component of dislocations can be resolved using HREM. Because the ⟨111⟩ screws do not meet the second imaging requirement and because the majority of the $b=[001]$ dislocations have ⟨100⟩ line directions, HREM was carried out by imaging crystals with the beam direction along [100] and [010] orientations.

3.2.1. Fe–40at.%Al

Interestingly, HREM of Fe–40at.%Al revealed not only $b_2=\langle 001\rangle$ dislocations, but also dislocations with $b_2=\langle 110\rangle$. Fig. 4 shows a HREM image of a $b=[001](100)$ edge dislocation. This image (and all of the other HREM images in this paper) is a "white atom" image with the bright spots representing approximate atomic positions. Despite the fact that the dislocations may not be moving by slip, for purposes of discussion, the "slip plane" will be defined as the plane which contains the Burgers vector and the dislocation line direction. Fig. 4 also displays a series of digitally compressed experimental images which help to illustrate the displacements in various directions and the termination of atomic planes. The core presented in Fig. 4 can be characterized by two distinct {220} half planes which terminate at approximately the same point (indicated by the arrows in Fig. 4(a)). These "extra half planes" can be seen more clearly in the compressed images shown in Figs. 4(b) and 4(d). This core is compact with only minimal spreading in the (100) slip plane (as revealed in Fig. 4(c)) and no significant distortions perpendicular to the slip plane (Fig. 4(e)). The compact nature of this core is very similar to that observed in Ni–50at.%Al and Ni–48at.%Al [23,24].

The second type of dislocation core observed in Fe–40at.%Al has an edge component of $b_2=[101]$ (as illustrated by the Burgers circuit in Fig. 5(a)). The Burgers vector analysis did not reveal any dislocations characterized by $b_2=[101]$ and $u=\langle 010\rangle$. Therefore it is not entirely clear how this dislocation relates to the deformation substructure. An interesting aspect of this

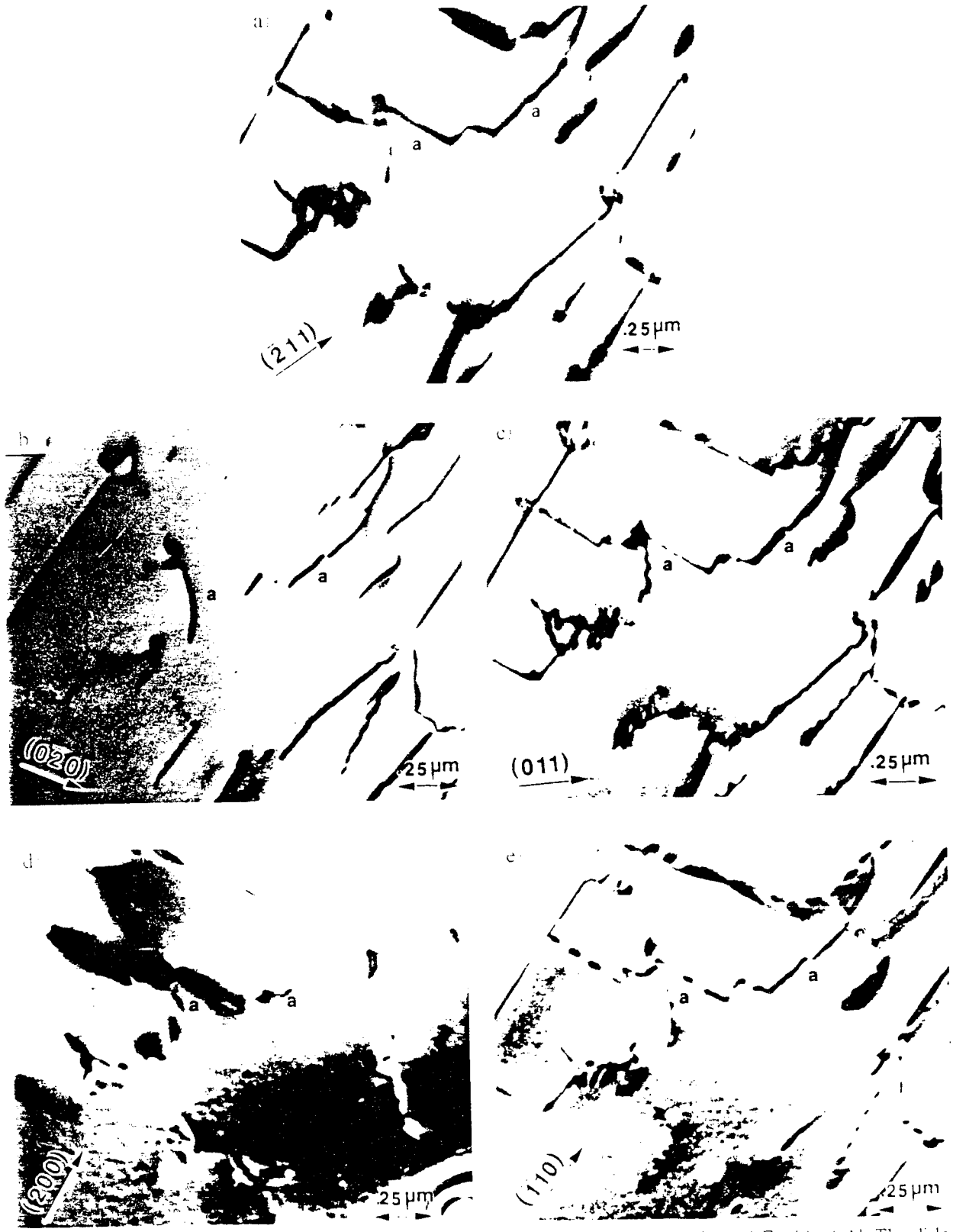

Fig. 2. Conventional diffraction contrast images illustrating a Burgers vector analysis in deformed Fe–40at.%Al. The dislocation labeled 'a' has a Burgers vector of [001] and line directions of [100] and [010], indicating that it is in a prismatic configuration. (a), (c) and (d) were taken near the [011] zone, while (b) and (e) were taken near [001].

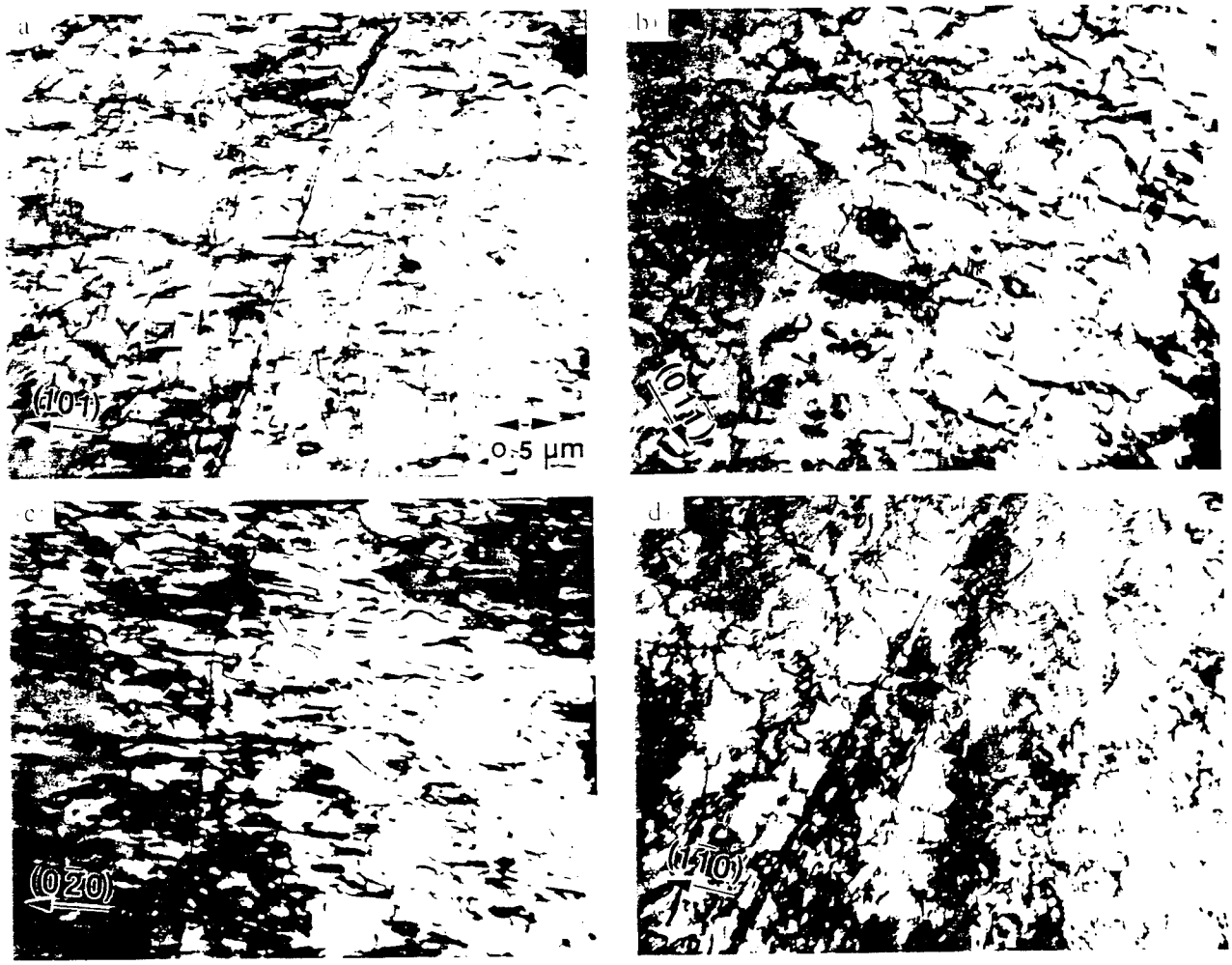

Fig. 3. Conventional TEM images of the deformation structure of Fe–50at.%Al deformed at 873 K. The substructure is dominated by ⟨100⟩ dislocations. The long straight dislocation is a ⟨111⟩ dislocation. a was taken near the ⟨010⟩ zone, b and c near ⟨111⟩ and (c) near ⟨001⟩.

dislocation core is that it is clearly dissociated into two dislocations with $b_p = \frac{1}{2}\langle 101\rangle$. These partials are separated by six interatomic spacings normal to the plane of the Burgers vector. This configuration, which appears to be the result of climb dissociation, can be clearly seen in the compressed image in Fig. 5a). Because $\frac{1}{2}\langle 110\rangle$ is not an atom to atom translation in the B2 structure, it is likely that the partial dislocations in this core have screw components and are most probably $\frac{1}{2}\langle 111\rangle$ dislocations coupled by an APB. Because it is not possible to determine the exact nature of the screw component of this perfect dislocation, it is necessary to consider various dissociation possibilities. The following dissociation schemes are the two most probable reactions. First, if the perfect dislocation is $b = \langle 101\rangle$, the dislocation may dissociate according to

$$\langle 101\rangle = \tfrac{1}{2}\langle 111\rangle + \mathrm{APB} + \tfrac{1}{2}\langle 1\bar{1}1\rangle$$

Second, if the perfect dislocation is $b = \langle 111\rangle$, the dislocation may dissociate by the reaction an equivalent reaction would occur for $b = \langle 1\bar{1}1\rangle$

$$\langle 111\rangle = \tfrac{1}{2}\langle 111\rangle + \mathrm{APB} + \tfrac{1}{2}\langle 111\rangle$$

In either case, the dissociation has occurred normal to the slip plane. Fig. 5b) shows the same dislocation following a few minutes exposure to the beam. In this figure, the lower partial dislocation has slipped relative to the upper partial in the direction of the Burgers vector. The partials lie on planes, six vertically separated glide planes apart, instead of lying nearly above one another, and are now separated by approximately four interatomic spacings in the direction of the Burgers vector. This motion requires the creation of additional APBs which will further restrict the slip of these partial dislocations.

3.2.2. Fe–50at.%Al

Only dislocations with $b_p = \langle 100\rangle$ were observed in the HREM studies of Fe–50at.%Al. However, a number of different core structures were observed.

The first of these structures (Fig. 6) is similar to that observed for the $b_c = \langle 100 \rangle$ dislocations in Fe–40at.%Al. It has a compact core characterized by the {220} extra half planes terminating very close to each other. However, careful examination reveals that these {220} terminations at the core in Fe–50at.%Al actually lie above one another relative to the slip plane. This suggests that some climb has occurred in this core, resulting in a somewhat non-planar core.

The second $b_c = \langle 100 \rangle$ core observed in Fe–50at.%Al (Fig. 7) reveals the {220} half plane terminations to be more widely spread (approximately 10–12 atom positions) in the {200} plane of the Burgers vector. This indicates a dissociation into two distinct partial dislocations. Fig. 7 displays the two $\frac{1}{2}\langle 110 \rangle$ Burgers circuits. In terms of the edge components, this dissociation would be

$$[001]_c = \tfrac{1}{2}[\bar{1}01]_c + \tfrac{1}{2}[101]_c$$

However, $\frac{1}{2}\langle 110 \rangle$ is not an atom to atom translation in the B2 structure. Thus a more likely dissociation which would take into account screw displacements parallel with the electron beam would be

$$[001] = \tfrac{1}{2}[\bar{1}11] + \mathrm{APB} + \tfrac{1}{2}[1\bar{1}1]$$

Due to the fact that the $\frac{1}{2}\langle 111 \rangle$ partials do not lie in the {200} slip plane (the approximate plane of the dissociation), they could not have simply slipped on the {200} plane into the observed configuration. Instead, two possible mechanisms may be responsible for the dissociation as illustrated in Fig. 8. First, both $\frac{1}{2}\langle 111 \rangle$ partials could glide on perpendicular {220} planes from the position of the original perfect [001] dislocation.

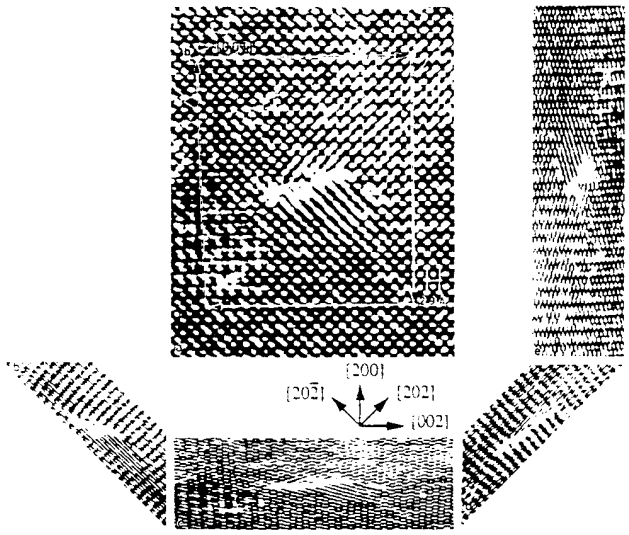

Fig. 4. (a) Experimental HREM image of a $\boldsymbol{b}=[001](100)$ edge dislocation in Fe–40at.%Al. (b–e) Digitally compressed representations of (a) corresponding to views down the [202] (b), [200] (c), [20$\bar{2}$] (d) and [002] (e) directions.

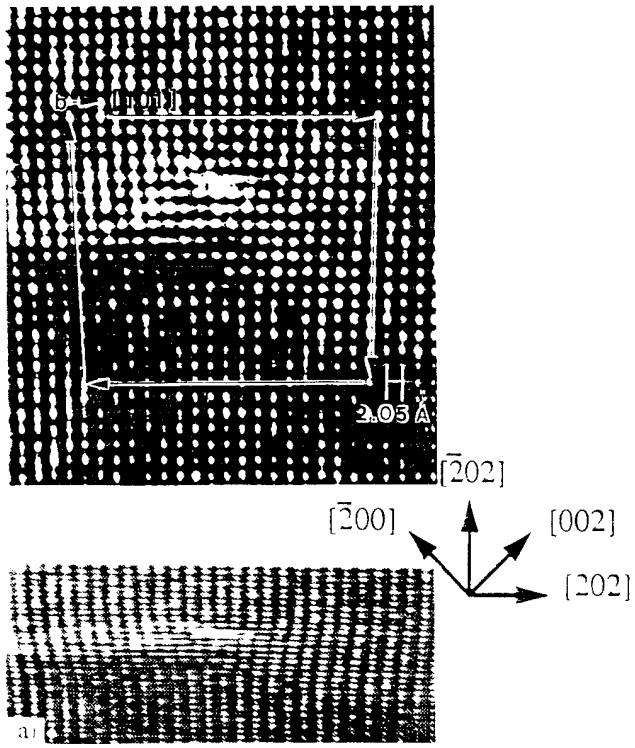

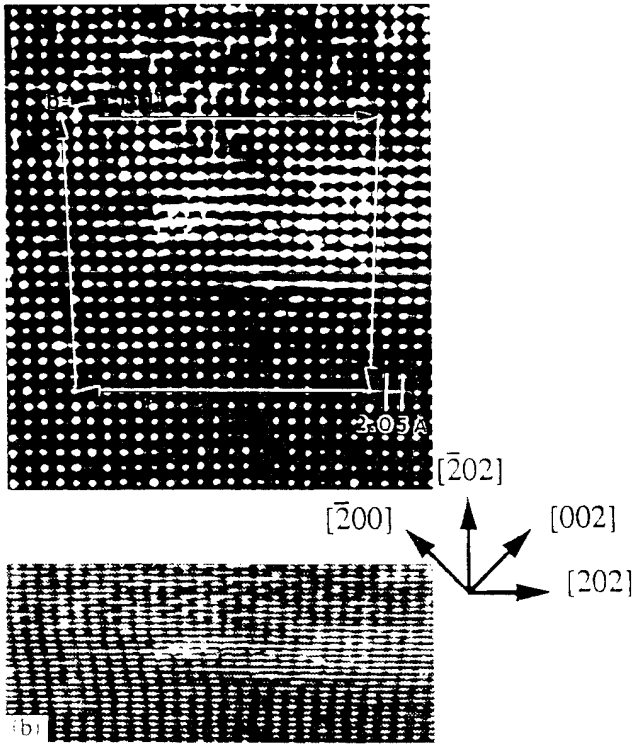

Fig. 5. HREM images of a climb dissociated dislocation core in Fe–40at.%Al with a $b_c = [101]$ edge component: (a) core in the initial configuration; (b) core following beam-induced slip of one of the partial dislocations.

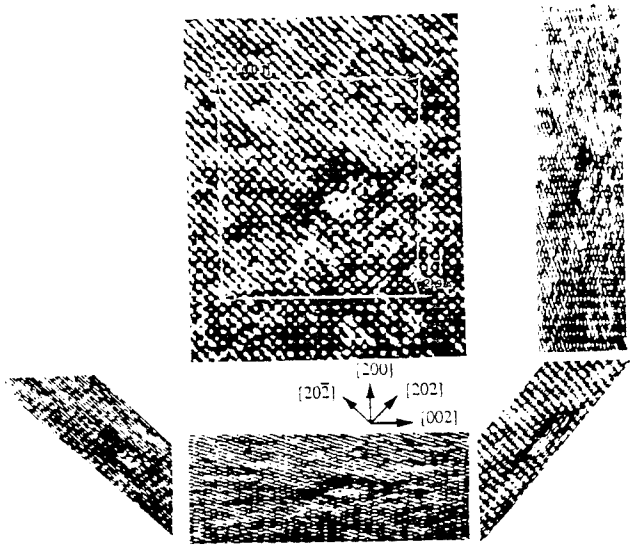

Fig. 6. Experimental HREM image of a compact {001}⟨100⟩ dislocation core in Fe–50at.%Al. Close examination shows that the {220} extra half planes denoted by arrows terminate at positions above one another relative to the plane of the total Burgers vector.

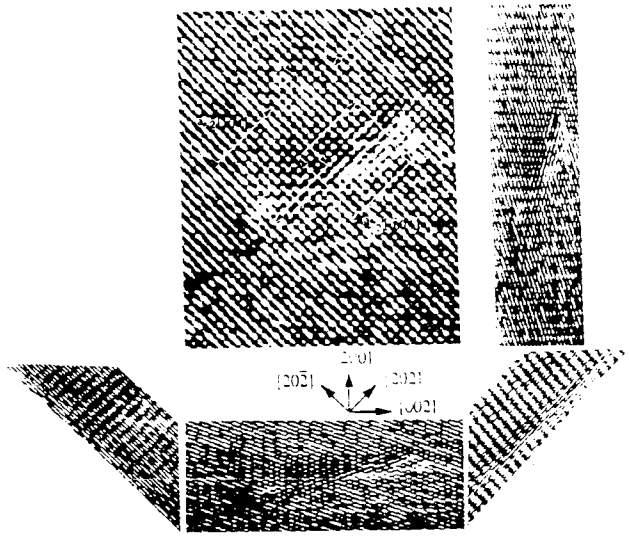

Fig. 7. HREM image of a dissociated ⟨001⟩{100} dislocation core in Fe–50at.%Al. The individual Burgers circuits indicate the direction of the edge component of the Burgers vectors of the partial dislocations.

This extends the APB in a V-shaped configuration. The dissociation configuration could also be a result of climb of the partials into a Λ-shaped configuration. However, as illustrated in Fig. 8, only negative climb the addition of atoms at the extra half plane can result in a structure completely consistent with that observed experimentally. It should be pointed out that the dissociation of a ⟨100⟩ dislocation into two ½⟨111⟩ partials is not expected to be energetically favorable when considering linear elasticity. However, this

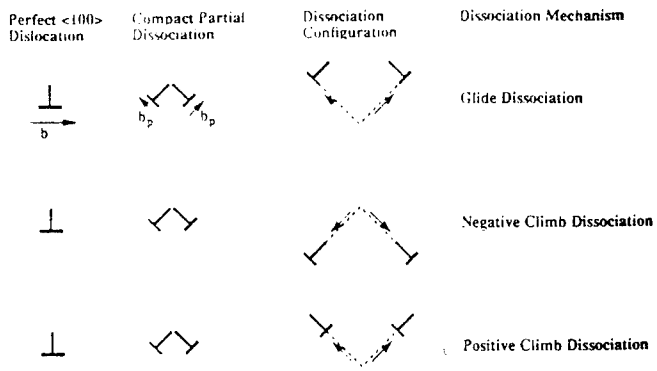

Fig. 8. Schematic representations of possible glide and climb mechanisms which could result in ½⟨111⟩ partials separated along a {100} plane. The broken lines represent an APB and the arrows note the direction of dislocation motion. Only glide dissociation and negative climb dissociation can result in a configuration consistent with Fig. 7.

Fig. 9. Experimental image of a dipole of two ⟨001⟩ dislocations in Fe–50at.%Al. The two dislocations lie approximately ten atomic planes apart in the ⟨100⟩ direction.

decomposition has been shown to be a mechanism for vacancy annihilation in Fe–42at.%Al by Fourdeux and Lesbats [6].

Fig. 9 shows two ⟨100⟩ dislocation cores in an apparent dipole configuration. The two cores (with opposite edge components) lie above one another with respect to the slip plane and are separated by approxi-

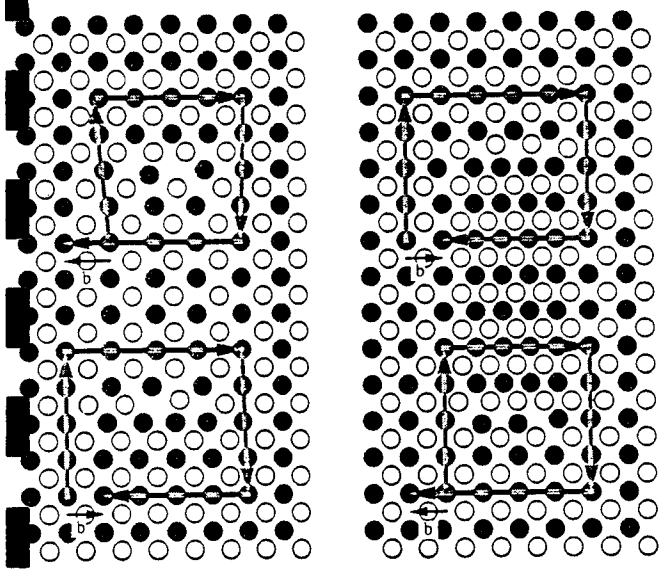

(a) (b)

Fig. 10. Schematic representation of (a) a vacancy dipole and (b) an interstitial dipole. The sense of the Burgers vector of the vacancy dipole is consistent with the experimentally observed image in Fig. 9.

mately ten interatomic spacings. For a dipole consisting of two edge dislocations, linear elasticity predicts that the two edge dislocations should lie 45° to each other. If the observed dislocations had interacted through slip, such a configuration would be expected. However, if the dislocations were a section through a dipole loop which formed through vacancy coalescence, the observed configuration may be expected. A comparison of Fig. 9 with Fig. 10 shows that the observed relationship between the Burgers vectors is in fact consistent with a vacancy dipole. This suggests that the observed structure may be a prismatic loop nucleus. Such a structure is consistent with previous observations of large numbers of ⟨100⟩ dipole loops in Fe–Al alloys deformed at high temperature [16,17,22]. Close analysis of the individual ⟨100⟩ dislocations in Fig. 9 shows that the arrangement of the {220} extra half planes is somewhat different in the two dislocations. This may suggest that the core structures of these dislocations vary somewhat during the climb process.

4. Discussion

The results show that there is a wide variety of dislocation core structures which can exist in B2 FeAl deformed at elevated temperatures. The observed structures may be indicative of configurations during slip at high temperature, or a result of rearrangement at elevated temperatures (with or without deformation) or during cooling following deformation. In particular, the discrepancy between the slip line observations (which indicated a well-defined {110} slip plane) and the diffraction contrast experiments (which found most of the dislocations to be in prismatic configurations) suggests that either a substantial amount of deformation is occurring through climb processes and/or the dislocations responsible for the slip lines undergo significant rearrangement following deformation. The furnace cooling of the compression samples may have allowed this rearrangement to take place.

The other point which must be considered when discussing the results is the role played by thermal vacancies. The very large number of vacancies which exist in Fe–Al alloys at high temperature (which can be retained at low temperature) may be interacting strongly with the dislocations. Again, the ⟨100⟩ prismatic dislocations suggest that significant climb processes are occurring and the high concentrations of thermal vacancies will clearly enhance this process. At the atomic level of the dislocations, vacancy incorporation will affect the core structure which may lead to non-planar core configurations. A number of core structures which indicate non-planar dissociations have been presented in this paper. Clearly, many of these non-planar structures will require reassociation in order to slip. This in turn may lead to difficulties in activating this slip.

While the core structures presented in this study have been produced at high temperature, the results may have implications for low temperature deformation and cooling rate effects. Quenched-in vacancy concentrations on the order of 10^{-3} suggest that only short-range vacancy motion is necessary for interaction between vacancies and dislocations. Furthermore, dislocations will encounter very large numbers of vacancies during slip. Although the active dislocations at low temperatures are different from those at high temperatures (⟨111⟩ vs. ⟨100⟩), it is reasonable to expect vacancies to interact with the dislocations involved in low temperature deformation in a manner similar to the interactions at higher temperatures. In other words, vacancy–dislocation interaction at low temperature (and in particular in rapidly cooled materials) may lead to the creation of non-planar core structures which may inhibit dislocation motion and lead to material strengthening.

5. Conclusions

Transmission electron microscopy of single-crystal Fe–40at.%Al and Fe–50at.%Al compressed at 873 K has revealed substructures dominated by ⟨001⟩{001} prismatic dislocations. Atomic resolution examination of the core structures of dislocations in these alloys

reveals a variety of core configurations. Compact cores in glide configurations have been observed as well as cores with non-planar structures. Some cores show significant evidence of climb dissociation. The results suggest that thermal vacancies which are present in large concentrations in these alloys may be interacting with the dislocations to produce non-planar core configurations. This may in turn lead to reduced dislocation mobility and material strengthening.

Acknowledgments

The authors would like to acknowledge the support of the Office of Naval Research through grant number N00014-90-J-1910 (Scientific Officer, Dr. G. Yoder). The Fe-40at.%Al single crystals were provided by Dr. R. Noebe of NASA LRC and Dr. S. Hartfield. The HREM was performed at the University of Michigan Electron Microbeam Analysis Laboratory (Director, Dr. J.F. Mansfield).

References

[1] Y. Umakoshi and M. Yamaguchi, *Philos. Mag. A, 41* (1980) 573.
[2] Y. Umakoshi and M. Yamaguchi, *Philos. Mag. A, 44* (1981) 711.
[3] D.J. Gaydosh and M.A. Crimp, *Proc. Mater. Res. Soc., 39* (1985) 429.
[4] M.A. Crimp, K. Vedula and D.J. Gaydosh, *Proc. Mater. Res. Soc., 81* (1987) 499.
[5] C.T. Liu, E.H. Lee and C.G. McKamey, *Scr. Metall., 23* (1989) 875.
[6] M.A. Crimp and K. Vedula, *Philos. Mag. A, 63* (1991) 559.
[7] M.G. Mendiratta, H. Kim and H.A. Lipsitt, *Metall. Trans. A, 15* (1984) 395.
[8] M.A. Crimp and K. Vedula, *Mater. Sci. Eng., 78* (1986) 193.
[9] J.R. Stephens, *Proc. Mater. Res. Soc., 39* (1985) 381.
[10] J. Rieu and C. Goux, *Mem. Sci. Rev. Met., 66* (1969) 869.
[11] J.P. Riviere and J. Grilhe, *Acta Metall., 20* (1972) 1275.
[12] D. Paris, P. Lesbats and J. Levy, *Scr. Metall., 9* (1975) 1373.
[13] D. Paris and P. Lesbats, *J. Nucl. Mater., 69* (1978).
[14] K.M. Ralls, T.M. Courtney and J. Wulff, *Introduction to Materials Science and Engineering*, Wiley, New York, 1976, p. 189.
[15] N. Junqua, J.C. Desoyer and P. Moine, *Phys. Status Solidi A, 18* (1973) 387.
[16] A. Fordeux and P. Lesbats, *Philos. Mag. A, 45* (1982) 81.
[17] N. Junqua, J.C. Desoyer and J. Grilhe, *Acta Metall., 30* (1982) 395.
[18] D. Weber, M. Meurtin, D. Paris, A. Foureux and P. Lesbats, *J. Phys. C7, 37* (1977) 332.
[19] M.A. Crimp and K.M. Vedula, *Mater. Sci. Eng., A165* (1993) 29.
[20] B. Schmidt, P. Nagpal and I. Baker, *Proc. Mater. Res. Soc., 133* (1989) 755.
[21] P. Nagpal and I. Baker, *Metall. Trans. A, 21* (1990) 2281.
[22] M.A. Crimp, *Ph.D. Dissertation*, Case Western Reserve University, 1987.
[23] M.J. Mills and D.B. Miracle, *Acta Metall. Mater., 41* (1993) 85.
[24] M.A. Crimp, S.C. Tonn and Y. Zhang, *Mater. Sci. Eng., A170* (1993) 95.

CHARACTERIZATION OF DEFORMATION STRUCTURES IN B2 CoAl

M.A. Crimp and Y. Zhang
Michigan State University, Department of Materials Science and Mechanics, East Lansing, MI 48824-1226

ABSTRACT

B2 CoAl single crystals with a number of orientations have been deformed at 1300 K and 1000 K. The deformation substructures have been characterized using TEM diffraction contrast techniques supported by image simulations. While <100> slip is found to be the predominant slip mode at these temperatures, <111> and <110> dislocations have also been observed. In particular, in hard orientations <110> dislocations appear to play an active role in initiating the deformation. Additionally, <110> dislocations are often observed as junctions of <100> type dislocations. Under the conditions tested, changes in alloy stoichiometry do not result in any modifications to the dislocation slip behavior.

INTRODUCTION

Over the past decade, there has been extensive research examining a wide range of intermetallic alloys, with a significant portion of this work focused on the B2 aluminides. In this class of materials, NiAl has received the bulk of the attention, with FeAl also the subject of considerable work. For example, volume V of this symposium[1] lists 38 papers focused on NiAl with another 7 devoted to FeAl. In contrast, the third transition metal aluminide, CoAl, has received little attention in the literature. This may be due to the reputation CoAl has for extreme brittleness. However, a number of studies[2-4] have shown that CoAl has significantly greater high temperature creep strength than either NiAl or FeAl. This is despite the finding that CoAl and NiAl have similar self diffusion rates at these high temperatures[2]. One possibility for the enhanced strength of CoAl may be differences in the dislocation slip behavior with the other B2 aluminides.

The dislocation behavior has been studied extensively in both NiAl (for review see [5]) and FeAl[6-9]. In NiAl, slip generally occurs through the motion of <100> dislocations on either {001} or {011} planes at both low and high temperature. <111> slip can normally only be activated below ambient temperature or by orienting single crystals to "hard" orientations. In contrast, B2 FeAl deforms exclusively by <111> slip at low to moderate temperatures, with a distinct transition to <100> slip at higher temperatures.

Unlike NiAl and FeAl, dislocation observations have been extremely limited for CoAl. The first imaging of dislocations in CoAl was reported by Hocking, Strutt and Dodd[2] who studied creep deformed single crystals. Although no analysis was performed, this group assumed the dislocations were <100> as the observed structures were very similar to those observed in NiAl. However, <111> edge dislocations have been reported in addition to <100> edge dislocations in polycrystalline Co-49.3at%Al extruded at 1505 K[10,11]. Somewhat surprisingly and in contrast to NiAl, Dreiles[12] found that <111> slip dominated the deformation of single crystals at ambient temperature. Only in crystals oriented near [111] were <100> dislocations activated. In [011] oriented single crystals the present authors[13] found only <100> edge and screw dislocations in stoichiometric, Co-rich and Al-rich alloys deformed at 673 K.

J. Horton et. al. eds., MRS Proceedings, Vol. 364 (1995) (in press).

As the dislocation structures in single crystal CoAl have been characterized at low to moderate temperatures, the purpose of the present study is to characterize the dislocations which are involved in the high temperature deformation of CoAl. To this end, oriented single crystals of CoAl with Co-rich, stoichiometric and Al-rich chemistries have been studied.

EXPERIMENTAL PROCEDURES

The materials used in this study were single crystals of B2 CoAl with compositions Co-50at.%Al (hereafter Co-50Al), Co-48Al, and Co-52Al. Nominally 3x3x9 mm compression samples were electro-discharge machined (EDM) from crystals which had been oriented using back-reflection Laue. The compression samples were mechanically ground and electro-polished to remove any surface damage. Deformation was performed in vacuum at 1300 K (one specimen was deformed at 1000 K) at a nominal strain rate of $2x10^{-4}$ to approximately 5% plastic strain. 3mm disks cut from oriented sections were electropolished for TEM observation in a twin jet polisher at -30°C with an 8% perchloric acid in methanol electrolyte and a voltage of 10 V.

Dislocation structures were characterized using standard diffraction contrast methods ($\mathbf{g}\cdot\mathbf{b}=0$ and $\mathbf{g}\cdot\mathbf{b}\times\mathbf{u}=0$ methods). However, because of the elastic anisotropy of CoAl, the results of these studies were at times inconclusive. Thus in order to confirm the analyses, image simulations were performed using the method of Head et. al.[14]. The details of the input parameters for these simulations are given elsewhere[15].

RESULTS AND DISCUSSION

The dislocation substructure was characterized in the various CoAl alloys with orientations of $[\bar{1}23]$, [011] and [011] deformed at 1300 K, and in one additional [011] oriented Co-50Al sample compressed at 1000 K (see Table I). Space constraints prevent the presentation of a detailed analysis of all of these conditions. However, a representative analysis will be presented along with summaries of the general effects of variations in stoichiometry, crystal orientation and deformation temperature.

An analysis of the deformation substructure for the $[\bar{1}23]$ oriented Co-50Al deformed at 1300 K is presented Fig. 1. While the structure is characterized by a relatively low dislocation density, the dislocations which are present have a wide variety characteristics including a number of different Burgers vectors and orientations. Dislocations with three different Burgers vectors, examples of which are labeled a, b, and c in Fig. 1, have been identified. In general, the majority of the dislocations were the type labeled c, with smaller numbers of type a and b dislocations. The dislocations labeled a have a general line direction of [100] and display weak contrast for $g=(\bar{2}00)$ and $(\bar{2}11)$,

Table I. Combinations of CoAl Alloy Stoichiometry, Deformation Temperature, and Crystal Orientations Characterized by TEM.

Co-50Al	$[\bar{1}23]$	1300 K
"	$[\bar{1}23]$	1000 K
"	[001]	1300 K
"	[011]	1300 K
Co-52Al	[011]	1300 K
Co-48Al	[011]	1300 K

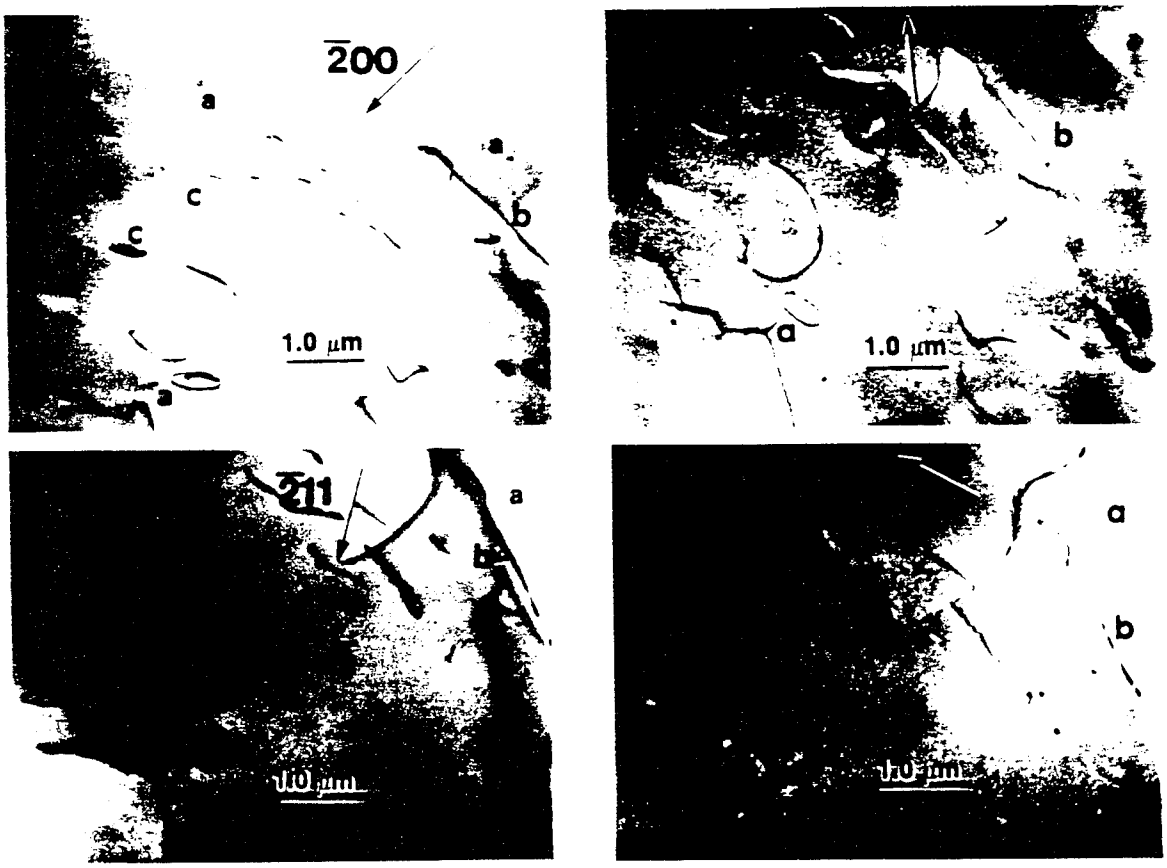

Figure 1. TEM bright field images of dislocations generated in [$\bar{1}$23] oriented Co-50Al deformed at 1300 K.

indicating a Burgers vector of **b**=[01$\bar{1}$]. These dislocations were observed both as isolated dislocations and as part of dislocation reactions. Figure 2 shows an indexed junction of two <100> dislocations interacting to form a <110> dislocation by the following reaction:

$$a[001] + a[010] = a[011]. \qquad (1)$$

Conversely, this may actually be a decomposition of a <110> dislocation into two <100> dislocations. It was not possible to obtain significant invisibility for more than one reflection for either dislocations b or c. For example, dislocations b display weak, dotted contrast for **g**=(1$\bar{1}$0) and dislocations c are out of contrast for **g**=(0$\bar{1}$1), but neither dislocation type is clearly invisible in the other figures. Thus it was necessary to use image simulation to fully characterize these dislocations. Figure 3 displays a series of simulations related to the imaging of dislocations b. Analysis of this figure leads to the conclusion that dislocations b have **b**=[$\bar{1}$11] and are mixed in character lying on the ($\bar{1}$01) plane. This conclusion is consistent with the limited invisibility observed for these dislocations. It should be noted that the experimental and simulated images do not match perfectly because the experimental dislocations are not entirely isolated from other dislocations and because the actual dislocation lines are not entirely straight. Dislocations c are simulated in fig. 4. These dislocations, which are in the majority, are found to have **b**=[100] and are edge in character. Thus, a complete analysis of Co-50Al deformed in the [$\bar{1}$23] orientation at 1300 K reveals a mix of dislocations including <100>, <110> and <111> dislocations.

While the above analysis outlines the general nature of the dislocations observed in this

study, it is worth noting the effect of various experimental parameters on this behavior. In particular, it should be pointed out that <111> dislocations were not observed under any other conditions.

Effect of Crystal Orientation

The effect of the orientation of the deformation axis on the nature of the dislocations was examined by varying the deformation axis to (011) and (001) for the stoichiometric Co-50Al deformed at 1300 K. In the (011) orientation, the Schmid factor (see table II) on the <100>{010} slip systems is maximized, and this is reflected in activation of both **b**=[100] and **b**=[010] edge

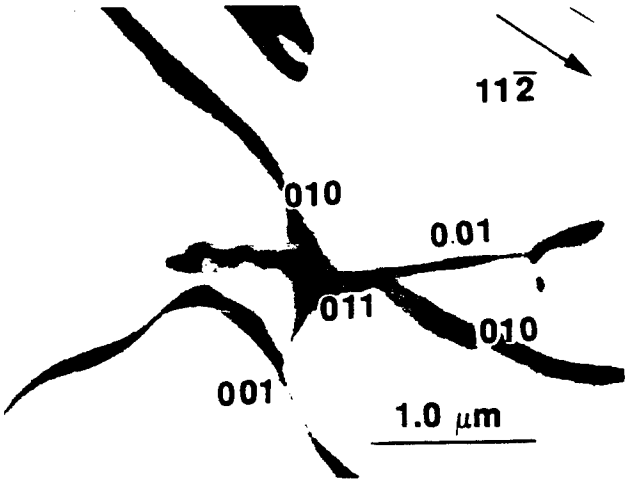

Figure 2. Detail of a dislocation reaction observed in [$\bar{1}$23] Co-50Al deformed at 1300 K.

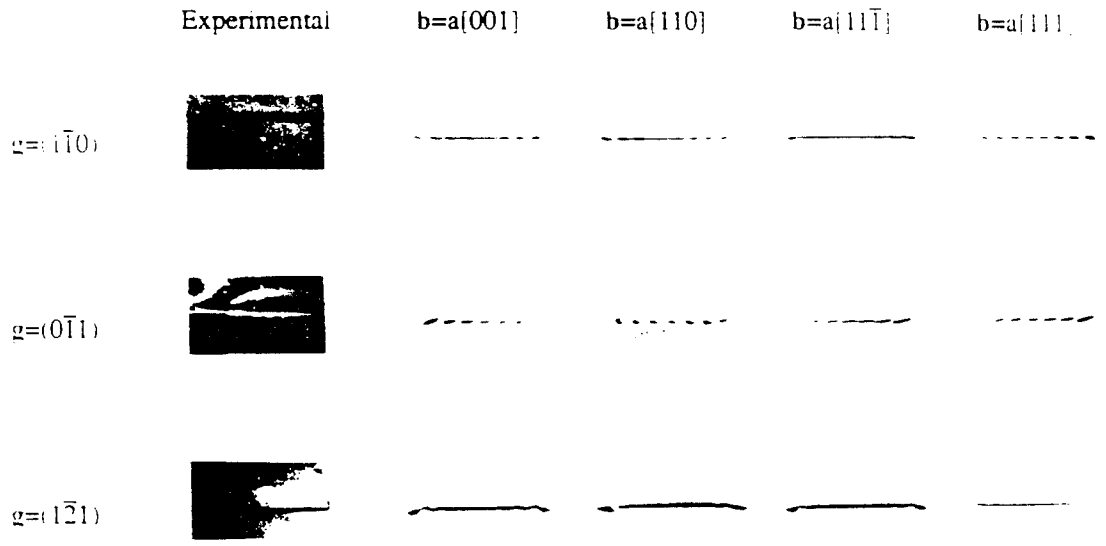

Figure 3. Experimental and simulated images of **b**=[111] dislocation in [$\bar{1}$23] oriented Co-50Al deformed at 1300 K.

dislocations. Some prismatic {001} loops are also observed. Consistent with the lower Schmid factors on other slip systems, no <111> dislocations are observed in this orientation. However, unlike the observations at 673 K, small numbers of <110> dislocations were observed as part of dislocation junctions. When the deformation axis is changed to (001), the structure is characterized by areas in which **b**=[100] and **b**=[0$\bar{1}$0] edge dislocations are the predominant dislocation, and other areas where **b**=[011] and **b**=[$\bar{1}$01] edge dislocation are in the majority. Overall, the density of <110> dislocations is much larger in this orientation. A possible explanation for this interesting deformation structure is that in the (001) orientation, the Schmid factor for <100>{010} slip is extremely low. Hence it is possible to activate slip of <110> dislocations, despite the fact they may have higher critical resolved shear stresses. However, as deformation continues, the crystal orientation rotates away from [001], leading to the activation

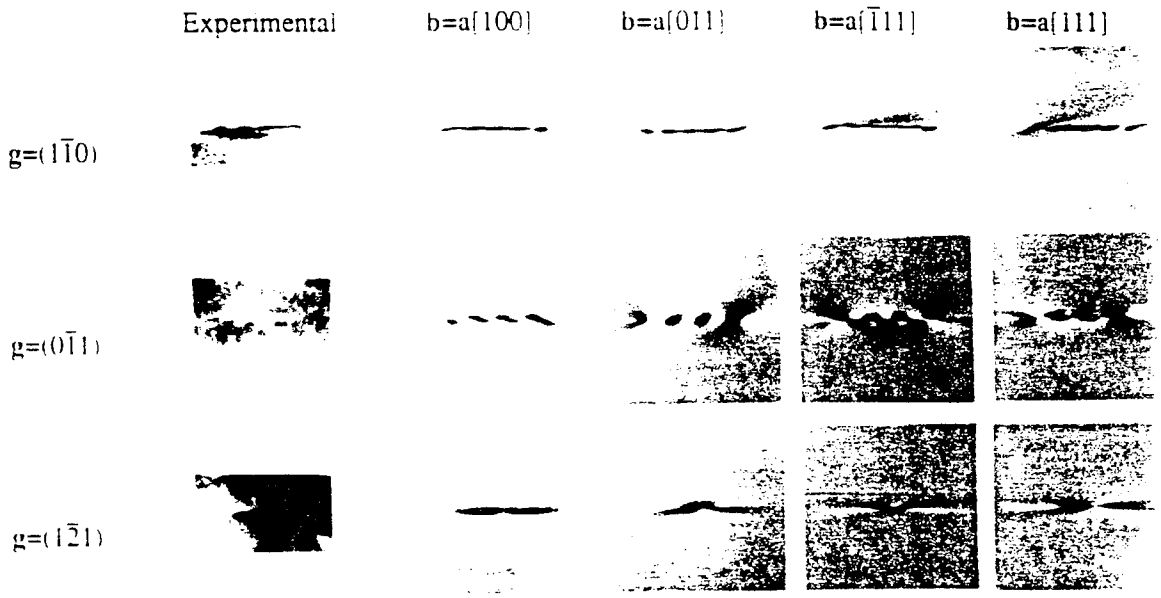

Figure 4. Summary of image simulations for **b**=[100] dislocations.

of <100>{010} as the Schmid factor increases. Consistent with this explanation, kinking of the [001] samples was observed. An interesting observation is that many long <110> dislocations are involved in junctions with <100> dislocations. It may be that as <100> slip becomes more favorable, the <110> dislocations decompose to lower energy/lower critical resolved shear stress <100> dislocations. Such decomposition has been observed in NiAl[16-17].

Effect of Co-Al Alloy Stoichiometry

The effect of alloy stoichiometry was studied by examining [011] oriented alloys with 48, 50 and 52Al deformed at 1300 K. In all of these alloys, <100>{010} edge dislocations were the predominant dislocation type, but short <110> dislocations involved in junctions of <100> were again observed. In contrast, only <100>{010} slip was observed for the same materials deformed at 673 K in this orientation in a previous study[13]. The dominance of <100> dislocations in these alloys may be a consequence of the selection of [011] as the deformation axis. As substantial <110> and limited <111> slip have been observed in this and other studies of CoAl alloys, it may be that selection of another orientation may result in significant activation of non-<100> slip in off stoichiometric CoAl single crystals.

Table II. Schmid Factors for the Observed Slip Systems and Experimental Compression Axes.

slip system	<100> {010}	<110> {112}	<111> {011}
Comp. Axis	S.F.	S.F.	S.F.
[001]	0.00	0.289	0.41
[$\bar{1}$23]	0.43	0.49	0.47
[011]	0.50	0.43	0.41

Effect of Deformation Temperature

In order to examine the effect of temperature, [$\bar{1}$23] oriented Co-50Al was deformed at 1000 K. In contrast to deformation in this orientation at 1300 K, no <111> dislocations were observed at 1000 K. The deformation structure is characterized by <100> dislocations and small numbers of <110> junctions. It is important to contrast

the results of the present study with those for deformation at 673 K. Clearly, deformation at 1000 K and 1300 K has resulted in significant numbers of <110> dislocations, particularly in the form of junctions. Such dislocations were not observed at 673 K.

Clearly, <100>{001} slip is the predominant high temperature deformation mode in these materials under a variety of conditions of alloy stoichiometry and crystal orientation. However, consistent with the observations in high temperature extruded polycrystalline CoAl[10-11], <111> and <110> dislocations have been observed. In particular, these secondary systems can be activated under conditions where the slip of <100>{001} dislocations are inhibited, such as hard orientations. As <100> is the dominant dislocation type, CoAl slips in a manner similar to NiAl at high temperatures. This is despite the much higher dislocation creep strength of CoAl[3-4]. The differences in high temperature strength between these two materials might simply be a result of differences in the stress necessary to move the <100> dislocations. This stress may in turn be controlled by the core structure of these dislocations. Recent work in our lab does indeed indicate there are differences in these structures and will be the subject of a later paper.

ACKNOWLEDGEMENTS

This work was supported by the Office of Naval Research, through grant #N00014-90-J-1910, Dr. G. Yoder contract monitor. CoAl single crystals were provided by Dr. D. Pope and Dr. W.J. Romanow at The University of Pennsylvania.

REFERENCES

1. *High-Temperature Ordered Intermetallic Alloys V*, edited by I. Baker, R. Darolia, J.D. Whittenberger and M.H. Yoo, Mater. Res. Soc. Proc., **288** (1993).
2. L.A. Hocking, P.R. Strutt, and R.A. Dodd, J. of Int. Met., 99, 98 (1971).
3. J.D. Whittenberger, Mat. Sci. and Eng., **73**, 87 (1985).
4. J.D. Whittenberger, Mat. Sci. and Eng., **85**, 91 (1987).
5. D.B. Miracle, Acta Met. Mater., **39**, 1457 (1991).
6. Y. Umakoshi and M. Yamaguchi, Phil. Mag. A, **44**, 711 (1980).
7. M.G. Mendiratta, H.M. Kim, and H.A. Lipsitt, Met. Trans, **15A**, 395 (1984).
8. M.A. Crimp and K. Vedula, Phil. Mag. A, **63**, 559 (1991).
9. P.R. Munroe and I. Baker, J. Mat. Sci, **24**, 4246 (1989).
10. D.L. Yaney, A.R. Pelton and W.D. Nix, J. Mat. Sci., **21**, 2083 (1986).
11. D.L. Yaney and W.D. Nix, J. Mat. Sci., **23**, 3088 (1988).
12. C.J. Dreiles, M.S. Thesis, Michigan Technological Univ., (1985).
13. Y. Zhang, S.C. Tonn and M.A. Crimp, *High-Temperature Ordered Intermetallic Alloys V*, edited by I. Baker, R. Darolia, J.D. Whittenberger and M.H. Yoo, Mater. Res. Soc. Proc., **288**, 379 (1993).
14. A.K. Head, P. Humble, L.M. Clarebrough, A.J. Morton, and C.T. Forwood, *Defects in Crystal Solids*, edited by S. Amelinckx, North-Holland, (1973).
15. Y.Zhang, Ph.D. Dissertation, Michigan State University (1995).
16. M.J. Mills and D.B. Miracle, Acta Metall. Mater., **41**, 85 (1993).
17. K.R. Forbes, U. Glatzel, R. Darolia, and W.D. Nix, *High-Temperature Ordered Intermetallic Alloys V*, edited by I. Baker, R. Darolia, J.D. Whittenberger and M.H. Yoo, Mater. Res. Soc. Proc., **288**, 45 (1993).